**Nagra**
Nationale
Genossenschaft
für die Lagerung
radioaktiver Abfälle

**Cédra**
Société coopérative
nationale
pour l'entreposage
de déchets radioactifs

**Cisra**
Società cooperativa
nazionale
per l'immagazzinamento
di scorie radioattive



# TECHNICAL REPORT 88-13

## A BOREHOLE FLUID CONDUCTIVITY LOGGING METHOD FOR THE DETERMINATION OF FRACTURE INFLOW PARAMETERS

CHIN-FU TSANG[1)]
PETER HUFSCHMIED[2)]

JANUARY 1988

[1)] Earth Sciences Division, Lawrence Berkeley Laboratory
Berkeley, California 94720
[2)] Nagra

Parkstrasse 23 5401 Baden/Schweiz Telephon 056/20 55 11

**Nagra**
Nationale
Genossenschaft
für die Lagerung
radioaktiver Abfälle

**Cédra**
Société coopérative
nationale
pour l'entreposage
de déchets radioactifs

**Cisra**
Società cooperativa
nazionale
per l'immagazzinamento
di scorie radioattive

# TECHNICAL REPORT 88-13

## A BOREHOLE FLUID CONDUCTIVITY LOGGING METHOD FOR THE DETERMINATION OF FRACTURE INFLOW PARAMETERS

CHIN-FU TSANG[1)]
PETER HUFSCHMIED[2)]

JANUARY 1988

[1)] Earth Sciences Division, Lawrence Berkeley Laboratory
Berkeley, California 94720
[2)] Nagra

Parkstrasse 23 5401 Baden/Schweiz Telephon 056/20 55 11

Der vorliegende Bericht wurde im Rahmen des gemeinsamen Projektes der Nationalen Genossenschaft für die Lagerung radioaktiver Abfälle (Nagra) und des Office of Civilian Radioactive Waste Managements des U.S. Department of Energy (DOE) am Lawrence Berkeley Laboratory (LBL), Berkeley, California, erstellt. Die Autoren haben ihre eigenen Ansichten und Schlussfolgerungen dargestellt. Diese müssen nicht unbedingt mit denjenigen der genannten Organisationen übereinstimmen.

Le présent rapport a été préparé au Lawrence Berkeley Laboratory (LBL), Californie, dans le cadre du projet commun à la Société coopérative nationale pour l'entreposage de déchets radioactifs (Cédra) et à l'Office of Civilian Radioactive Waste Management du Département de l'Enérgie des Etats Unis (DOE). Les opinions et conclusions présentées sont celles des auteurs et ne correspondent pas nécessairement à celles des organisations nommées.

This report was prepared as part of the Joint Project between the National Cooperative for the Storage of Radioactive Waste (Nagra) and the Office of Civilian Radioactive Waste Management of the U.S. Departement of Energy (DOE) at the Lawrence Berkeley Laboratory (LBL), Berkeley, California. The viewpoints presented and conclusions reached are those of the authors and do not necessarily represent those of the organisations mentioned.

Dieser Bericht erscheint auch als Bericht des LBL, gekennzeichnet als LBL-23096 und gleichzeitig mit der Nummer NDC-1 des gemeinsamen Projektes der Nagra und des DOE.

Ce rapport est également publié par le LBL sous le label LBL-23096, et sous le label NDC-1, dans le cadre du projet commun à la Cédra et au DOE.

This report is published also by LBL under report number LBL-23096 as well as under number NDC-1 of the Nagra/DOE cooperative project.

## ABSTRACT

It is of much current interest to determine the flow characteristics of fractures intersecting a wellbore in order to provide data in the estimation of the hydrologic behavior of fractured rocks. In particular the fluid inflow rates from the fractures into the wellbore are important quantities to measure. However often these inflows are at very low rates. In addition very often one finds that only a few percent of the fractures identified by core inspection and geophysical logging are water-conducting fractures, the rest being closed, clogged or isolated from the water flow system. A new developed to locate water-conducting fractures and obtain fracture inflow parameters by means of a time sequence of electric conductivity logs of the borehole fluid. The physical basis of the analysis method is discussed. The procedure is applied to an existing set of data, which shows initiation and growth of nine conductivity peaks in a 900-m section of a 1690-m borehole, corresponding to nine waterconducting fractures intersecting the borehole. We are able to match all nine peaks and determine the flow rates from these fractures. A discussions is given on the applicability of this technique in the context of a borehole testing program.

## RESUME

La détermination des quantités d'eau s'écoulant dans les fractures, qui recoupent un forage revêt un intérêt tout particulier pour la caractérisation hydraulique des roches fracturées. En général, le débit fourni au forage par de telles fractures est très faible. En outre, souvent seules quelques unes des fractures repérées sur carottes ou par diagraphie sont aquifères, les autres étant fermées, colmatées ou isolées du réseau d'écoulement.

Une nouvelle méthode est proposée ici pour localiser les fractures aquifères et en quantifier le débit. Cette méthode est basée sur le développement du profil de la conductibilité électrique du fluide, qui remplit le forage, au cours d'une phase de pompage. Les bases physiques sur lesquelles s'appuie la méthode d'interprétation sont explicitées.

La méthode a été appliquée à un ensemble de données récoltées sur un tronçon de 900 m en roche cristalline, dans le forage de Leuggern, au Nord-Ouest de la Suisse. A partir de la situation initiale, on voit se développer 9 pics de la conductibilité électrique, qui sont liés à des venues d'eau minéralisée à partir des fractures qui recoupent le forage. La méthode d'analyse permet de reproduire, par simulation, le développement des 9 pics, et d'y associer le débit d'écoulement et la concentration en sels dissous de l'eau souterraine. Pour valider la méthode, des recherches complémentaires sont proposées.

## ZUSAMMENFASSUNG

Die Ermittlung der Grundwasser-Fliessmengen in Klüften, welche ein Bohrloch schneiden, ist von grosser Bedeutung im Zusammenhang mit der hydraulischen Charakterisierung von Kluftnetzwerken. Zuflüsse von den Klüften in ein Bohrloch sind in der Regel sehr klein; dazu kommt, dass häufig nur ein kleiner Prozentsatz der an Bohrkernen und mit Hilfe geophysikalischer Methoden identifizierten Klüfte Wasser führt. Die restlichen Klüfte sind entweder geschlossen, gefüllt oder nicht mit dem wasserführenden Kluftnetzwerk verbunden. Eine neue Methode wird vorgeschlagen und ein entsprechendes Auswertungsverfahren entwickelt, welches erlaubt, die wasserführenden Klüfte im Bohrloch zu lokalisieren und die Zuflussmengen zu quantifizieren. Die Auswertung stützt sich auf Messungen der zeitlichen Aenderung der elektrischen Leitfähigkeit der Flüssigkeitssäule im Bohrloch. Die physikalischen Grundlagen des Auswertungsverfahrens werden diskutiert. Anschliessend werden Messdaten aus einem ca. 900 m langen Abschnitt des Kristallins im Bohrloch Leuggern der NAGRA analysiert. Die Messdaten zeigen das Entstehen und das Wachstum der elektrischen Leitfähigkeit. Diese können als Zuflüsse von salinärem Wasser aus Klüften in das Bohrloch interpretiert werden. Alle Peaks konnten mit dem theoretischen Modell nachsimuliert, die entsprechenden Zuflüsse und die Konzentrationen der gelösten Salze der Formationswässer quantifiziert werden. Für die Validierung der Methode werden ergänzende Versuche vorgeschlagen. Weitere Arbeiten mit dem Ziel, die hydraulischen Transmissivitäten der einzelnen Zuflusszonen mit dieser Methode zu bestimmen sind im Gang.

**TABLE OF CONTENTS** Page



LIST OF TABLES Page

## LIST OF FIGURES

# 1 INTRODUCTION

In the study of the hydrology of fractured rocks, it is important to know the fracture properties. Surface observations may be useful, but the more relevant observations are those made at the depths of interest. Such measurements are mainly carried out through boreholes or underground openings. In the case of boreholes various methods of studying fracture properties have been used. For example, a downhole televiewer can be used to map the fracture traces on the borehole walls and determine their density and orientations. However, it is well known that often these traces do not correspond to locations of water-conducting fractures. Hence, there is a need to (1) identify the location and (2) measure directly the hydraulic or flow properties of an identified water-conducting fracture or group of fractures intersected by the borehole.

Constant-pressure, constant-flow or pulse tests have been applied to packed intervals along a wellbore. Since many of the fractured rocks of interest are of low permeability, the flow from a packed interval can be very slow. This has necessitated the development of low-flow measurement tools and the use of long-term measurements involving many packed intervals tested one at a time. Packed-off test intervals are usually larger than individual water-conducting zones, thus leading to an uncertainty in the location of a water-bearing fracture. An alternative method is the measurement of inflow along the borehole from fractures without the use of packers, with the well flowing at a moderate rate. Borehole flowmeters (see e.g., Hufschmied, 1983; Omega, 1987; Bean, 1971) can in principle yield the inflow rate from individual inflow zones. Such a flowmeter log is often strongly affected by wellbore radius variations. Thus, a caliper log has to be run to calibrate the results. Also, there is a low flow rate limit below which the conventional flowmeter log is no longer useful.

The present paper describes a new method involving the use of a time sequence of electric conductivity logs of borehole fluid. The following section describes the logging procedure and the analysis method used. Next, analytic considerations are discussed to show the functional dependence and expected results for the short and long time limits. Then the numerical code used in the data analysis is introduced. A set of data from the Leuggern borehole from Switzerland is then described and our analysis method applied to evaluate the inflow characteristics. Finally, discussions are given on the range of applicability of this technique in the context of a well-test program.

## 2 FLUID CONDUCTIVITY LOGGING PROCEDURE

Consider the uncased section of a wellbore that intersects a number of flowing fractures. In general, the flowing fractures contain fluids with different chemical compositions and ion content, and hence different electric conductivities. The relationship between ion concentration and fluid electric conductivity is reviewed, for example, by Shedlovsky and Shedlovsky (1971), who give graphs and tables relating these two quantities. Hale and Tsang (1987) made a sample fit for the case of NaCl solution at low concentrations and obtained

$$\sigma = 0.187C - 0.004C^2$$

where $\sigma$ is the fluid electric conductivity in S/m and C is concentration of NaCl in kg/m$^3$. The formula is valid at a temperature of 20°C, and for values of C up to $\approx$ 6 kg/m$^3$ and values of $\sigma$ up to 1.1 S/m (or 11000 µS/cm). The quadratic term can be dropped if one is interested only in values of C up to $\approx$ 4 kg/m$^3$ and $\sigma$ up to 0.8 S/m (or 8000 µS/cm). In this case we have a convenient linear relationship between $\sigma$ and C:

$$\sigma(\mu S/cm) = \alpha C(kg/m^3) \qquad (1)$$

where $\alpha$ = 1870 (µS/cm) · (m$^3$/kg) and the units were chosen because in applications described later in the paper $\sigma$ is given in µS/cm .

Suppose the wellbore is first washed out with de-ionized water by passing a tube to the well bottom. There will be some residual ion content and associated electric conductivity. In the field data shown later in the paper, the residual electric conductivity turns out to be about 60 µS/cm, corresponding to a residual salinity concentration of 0.03 kg/m$^3$. Now let us produce from the wellbore at a flow rate Q. For three fractures we have a situation shown schematically in Figure 1. Note that the flow rates at different parts of the wellbore are different, being equal to the sum of all upstream inflow rates. At each fracture inflow point, the parameters characterizing the flow are $t_{oi}$, the time when the fracture fluid emerges at the wellbore; $x_i$, the location of the inflow point; $q_i$, the volumetric inflow rate; and $q_iC_{oi}$, the solute mass inflow rate, where $C_{oi}$ is the concentration of ionic solutes in the fracture fluid. Here we have assumed that generally $t_{oi}$ can be different for different fracture inflow points. This could be due to different initial hydraulic heads in these fractures or the specific borehole development and pressure history.

Figures 2-5 display schematically salinity distribution inferred from fluid electric conductivity distribution in the wellbore for a series of times.

Figure 2 shows the curves for early values of time. In this paper we assume that the wellbore cross section is small compared with its length, so that salinity or chemical concentration is uniform at each cross section. If there is no overall vertical upward flow in the wellbore and density effects can be neglected, one expects the salinity curves at each inflow point to be symmetrical about the inflow point (see formula in the next section). When the well is pumped at a given flow rate, a skewing of the curves is expected due to the upward flow in the wellbore, which is larger near the well top than near the well bottom.

Figures 3-5 show three possible sets of salinity curves for large time periods, all assuming very small borehole diffusivity. Figure 3 shows one possible set of results. At large times, the saturation salinity is given by

$$C_{max,i} = \frac{wC_w + q_i C_i}{w + \sum_{n=1}^{i} q_n} \tag{2a}$$

where $q_i$ is the inflow rate, with i = 1 corresponding to the deepest inflow point (i.e., most upstream), and w is the borehole flow rate from well-bottom with salinity, $C_w$. If the salinity curves from two inflow points i and i + 1 overlap, then $C_{max,i}$ is still given by (1), but $C_{max,i+1}$ is given by

$$C_{max,i+1} = \frac{wC_w + q_i C_i + q_{i+1} C_{i+1}}{w + \sum_{n=1}^{i+1} q_n} \tag{2b}$$

There is a step-jump at the location of the (i+1)-th inflow point when the salinity curve from i-th inflow reaches the (i+1)-th location. This is demonstrated in Figure 3 for three inflow points, with second and third inflow salinity curves interfering with each other.

At the limit of very large time periods, the expected salinity curves are shown in Figure 4. Here the step structure is prominent, with the $C_{max}$ value between the i-th and (i+1)-th inflow points given by

$$C_{max,i} = \frac{wC_w + \sum_{n=1}^{i} q_n C_n}{w + \sum_{n=1}^{i} q_n} \tag{3}$$

With diffusion, the step structure will be smeared out. Note that the results, equations (2) and (3), are independent of variations of wellbore radius.

Figure 5 shows a sequence of curves from early to later times. In this figure, the effect of having one of the three inflows starting much earlier than the other two is shown.

Thus, the procedure for fluid conductivity logging is as follows. After the wellbore fluid is replaced by de-ionized water, the well is produced at a low flow rate. Then a fluid conductivity logging probe is run through the well-bore and electric conductivity distribution recorded at several times. Care should be taken not to disturb the wellbore fluid to induce large scale disturbances. With the time sequence of fluid conductivity logs, the inflow characteristics of the fractures can then be determined. For the field case described later in the paper, the well is about 1690 m deep with the section under survey ranging from 770 to 1637 m below the surface. Each logging run took about an hour and five logs were taken at intervals of about 4 to 20 hours.

## 3 ANALYTIC CONSIDERATIONS

In this section three simple analytic solutions are described. They illustrate key issues encountered in carrying out the flow conductivity logging and analysis.

For the flow in the wellbore to be below the turbulence regime, the Reynold's number, R, is below the critical value of about 2000. It is well known (e. g., Roberson and Crowe, 1985) that for a wellbore

$$R = \frac{vd}{\nu} \tag{4}$$

where v is linear velocity in the wellbore, d is wellbore diameter and $\nu$ the kinematic viscosity of the fluid. For example, if the well diameter is d = 15 cm and wellbore flow rate is 10 l/min, implying a linear flow velocity of about $10^{-2}$ m/sec, the Reynold's number is about 1500 for room-temperature water. This is below the critical Reynold's number.

For early times, the salinity concentration is still localized near the inflow points, so that we may consider each inflow point by itself. Further, if we assume that the overall wellbore flow velocity is relatively small and has little effect on the salinity curves at these early times, the problem is then equivalent to release of a chemical beginning at time, t = 0, at a given point, x = 0, say, in a linear pipe of stationary water, and an analytic solution is available. An important parameter

here is D, the molecular diffusion parameter associated with the spread of the chemical after it enters the pipe. If the mass inflow rate is $qC_o$, where q is flow rate in $m^3/s$ and $C_o$ is concentration of inflow fluid in $kg/m^3$, and d is wellbore diameter in meters, the solution is given by (see e.g., Fischer et al., 1979).

$$C(x,t) = \frac{qC_o}{\sqrt{4\pi D}} \cdot \frac{4}{\pi d^2} \cdot \int_0^t \frac{1}{\sqrt{t-\tau}} \exp\left[-\frac{x^2}{4D(t-\tau)}\right] d\tau \qquad (5)$$

A plot of this is shown in Figure 6. Several interesting properties of this expression that will be useful later are pointed out here. First, at the inflow point, x = 0, we find the following expression for peak height:

$$C(0,t) = \frac{qC_o}{\sqrt{\pi D}} \cdot \frac{4}{\pi d^2} \cdot \sqrt{t}$$

so that

$$[C(0,t)]^2 = \frac{(qC_o)^2}{\pi D} \cdot \frac{16}{\pi^2 d^4} \cdot t \qquad (6)$$

This shows that $[C(0,t)]^2$ is linearly dependent on t for early times and the slope of $[C(0,t)]^2$ versus t is $S_c = 16(qC_o)^2/\pi^3 D d^4$. If the release of chemicals at the wellbore begins at $t = t_o$, the formula can be easily modified to show that a plot of $[C(0,t)]^2$ versus t should have an x-intercept at $t_o$. Ideally, $t_o$ for all the inflow points should be the same, equal to the time when pumping starts. However they can be different if the fractures are at different initial hydraulic potentials relative to the wellbore, or if there are operational problems in pumping de-ionized water into the wellbore to establish initial conditions. Furthermore, if we calculate the area under the salinity curves at these early times, we obtain

$$\int C(x,t)dx = (qC_o) \cdot \frac{4}{\pi d^2} \cdot t \qquad (7)$$

as one would intuitively expect. Now a plot of $\int C(x,t)dx$ versus t will give a slope of $S_A = 4qC_o/\pi d^2$. Then, the ratio $S_A^2/S_c$ is just $\pi D$, a constant. The validity of the early time data can be checked by comparing this ratio for a number of inflow points in the same wellbore. Thus, by these simple considerations, one can obtain from early time curves both $t_o$ and $(qC_o)$.

In principle, once $t_o$ and $qC_o$ are obtained for each peak, one can apply large-time results, equations (1)-(3), to calculate the flow rate of the particular inflow point. Thus, from careful measurements of early-time log data and late-time log data, one can obtain all the inflow flow rates in a simple and straightforward way. These results are not sensitive to moderate variations of wellbore diffusivity. Note also that while the short-term results depend on welbore radius, the large-time results (equations 1-3) are independent of it.

Another analytic solution is available for the case where the inflow is well established and the wellbore flow dominates the movements of the inflow salinity. This corresponds to the problem of a continuous inflow at constant $qC_o$ at $x = 0$. Here

$$K\frac{\partial^2 C}{\partial x^2} - v\frac{\partial C}{\partial x} = \frac{\partial C}{\partial t} \tag{8}$$

with

$$C(x,t) = 0 \quad \text{at} \quad t = 0$$

$$\frac{\partial C}{\partial x} = 0 \quad \text{at} \quad x = \infty$$

and

$$C(0,t) = C_o \qquad \text{for } t > 0$$

In these equations v is the linear velocity given by q divided by the wellbore cross section area, and K is the asymptotic mechanical dispersion coefficient in a linear pipe, which is well studied by Taylor (1953), Aris (1956) and others. These authors found

$$K = \frac{d^2 v^2}{192D} \tag{9}$$

where d is the wellbore diameter, v is the linear flow velocity and D is the molecular diffusivity. Note that the boundary condition $C(0,t) = C_o$ for $t > 0$ in the constant linear flow stream with velocity v implies a constant solute release of $vC_o$ at $x = 0$. However not all solute flows up the borehole; there is a small amount ($K\partial C/\partial x$) that is diffused down the borehole (see equation (8) and Javandel et al. 1984).

The solution of the above differential equation (see e.g., Ogata and Banks, 1961) is

$$\frac{C}{C_o} = \frac{1}{2}\,\mathrm{erfc}\left[\frac{x-vt}{2\sqrt{(Kt)}}\right] + \frac{1}{2}\exp\left[\frac{vx}{K}\right]\mathrm{erfc}\left[\frac{x+vt}{2\sqrt{Kt}}\right] \qquad (10)$$

A plot of this solution is shown in Figure 7. One sees the steady migration of the salinity curves downstream, eventually saturating the whole wellbore with fluid of concentration $C_o$.

## 4 NUMERICAL METHOD

For a general problem of multiple inflow points, overlapping salinity curves and variable dispersion coefficient K, no analytic solution is readily available and numerical methods are required. For our purpose, we developed a simple computer code (Hale and Tsang, 1987) that solves the linear advective-dispersive equation:

$$K\frac{\partial^2 C}{\partial x^2} - v\frac{\partial C}{\partial x} + S = \frac{\partial C}{\partial t}$$

where C is the concentration of solute, K is the dispersion coefficient, v is the linear borehole fluid velocity, and S is the source term, under the initial condition:

$$C(x,0) = C_o(x) \qquad x \le x_{max},\ t = 0\ .$$

Here $x_{max}$ represents the deepest point of interest in the borehole. The code uses a finite difference solution scheme with upstream weighting and can accommodate various boundary conditions. It has been verified against a number of analytic solutions and also against a well-validated numerical code, PT (Bodvarsson, 1982; Tsang 1985; Tsang and Doughty, 1985). It is available on PC-diskette (Hale and Tsang, 1987).

In this section we shall present a few results of fluid salinity behavior in the wellbore to confirm the earlier schematic and analytic considerations and to study parameter sensitivities. In the next section on field experiments and data, we shall apply the code with actual parameters to analyze the data and evaluate the inflow parameters.

Figure 8 shows the numerical results of a case with one inflow point under an overall inflow flow rate w. It is apparent that at early times, the salinity peak grows in a way similar to the early time analytic

solution given by equation (5) (Figure 6). At later times, after the salinity value saturates to the inflow fluid salinity, the behavior is similar to that given by the late-time analytic solution, equation (10) (Fig. 7).

Figure 9 shows a late-time numerical solution for the case of the overall wellbore fluid flow rate w equal to 0, q/3 or q, where q is the fracture inflow rate. The saturation salinity values are $C_o$, 3/4 $C_o$ and 1/2 $C_o$ respectively. This is obvious from the proportionate mixing of inflow salinity with the upcoming wellbore flow with $C_w = 0$ (equation 1). Note that we are using the volume flow rates w and q and not linear velocities. Thus, the variation of wellbore cross-section has no effect on these results.

Figures 10a and 10b show the salinity curves in the wellbore for two different values of wellbore dispersivity, K. Here we assume that w = 0. Because there is a closed boundary at well bottom x = 0, there is still a preferred flow upwards to -x values. With inflow at rate q at the point x = -50 m, the flow rate in the wellbore is q downstream from x = -50 m and 0 upstream. In Figure 10a the value of K is 6.25 x $10^{-6}$ $m^2/s$, and in Figure 10b it is doubled. The curves display only small differences from each other, indicating low sensitivity to moderate uncertainties in K values.

Figures 11-13 show the interference between two inflow points. In all of these cases K is taken to be 1.25 x $10^{-5}$ $m^2/s$ and the overall wellbore flow rate to be w = 1.5 x $10^{-7}$ $m^3/s$. The two inflow points are at x = -50 m and x = -100 m with flow rates $q_1$ = 1.5 x $10^{-7}$ $m^3/s$ and $q_2$ = 3 x $10^{-7}$ $m^3/s$ respectively (Figure 11). Interference effects are seen when the salinity curve from the upstream inflow point overlaps the downstream point. Interference is drastically increased if the upstream inflow rate $q_1$ is doubled to $q_1$ = 3 x $10^{-7}$ $m^3/s$ (Figure 12). Figure 13 shows the large time period results with the upstream inflow (at x = -50 m) arbitrarily assumed to have a later starting time than the downstream inflow point (at x = -100 m ). The step structure at large times confirms that shown in Figure 4.

## 5 FIELD EXPERIMENT AND DATA ANALYSIS

The Leuggern borehole is one of six boreholes conducted by Nationale Genossenschaft für die Lagerung radioaktiver Abfälle (NAGRA) as part of a regional investigation program in Northern Switzerland. As shown on Figure 14, the borehole is located near the confluence of the Rhine and Aare Rivers in the Table Jura south of the Black Forest Massif. Drilling of the borehole began in June 1984, and was completed in February 1985, at a total apparent depth along the borehole of 1688.9 m. The borehole deviates slightly from vertical and thus, the true

terminal depth of the borehole below ground surface is 1631.6 m. In this paper, depth is measured along borehole.

The geology intersected by the borehole is described in Figure 15. A thin layer of unconsolidated quarternary deposits is underlain by consolidated Triassic sediments consisting of the Muschelkalk and Buntsandstein. The base of the Buntsandstein group lies unconformably on crystalline rock consisting of biotitegneiss to a depth of 1387.3 m and biolite-granite from 1387.3 m to 1688.9 m.

The Leuggern borehole contains various diameter casings to various depths. Of interest here is the final casing of 0.17 m diameter which was cemented to a depth of 557.5 m in the crystalline rock. Nominal borehole diameter below the casing is 0.14 m down to the final depth. Detailed information is provided by a caliper survey.

A suite of investigations was conducted in the borehole, including core logs, geophysical logs, hydraulic packer testing and hydrochemical sampling. A brief overview of the standard testing program in the NAGRA deep boreholes in Northern Switzerland and results are provided by Thury and Gautscchi (1986).

Fluid logging experiments were carried out by NAGRA in different boreholes during 1985. Measurements from the Leuggern borehole are taken as an example to demonstrate the applicability of the method. The Leuggern borehole extends 1689 m into crystalline bedrock. It was cased from the ground surface to a depth of 267 m, and a production-injection packer was set at 1637 m to shut off a highly permeable section near the bottom of the borehole. This was necessary to avoid a high flow rate through the low-permeability section, which would have covered up the very small inflow from this section. Only the section between 770 m and 1637 m was studied by the fluid log measurements. First the borehole water was replaced by de-ionized water through a downhole tubing, and the fluid conductivity was measured at the outflow at welltop to be 60 µS/cm. Then the tubing was pulled out of the well and the water level in the well was kept at zero by pouring de-ionized water into it. A pump was placed at -210 m, and background temperature and electric conductivity logs were taken. Then with pumping maintained at about 20 l/min a series of 5 complete electric conductivity logs were taken over two days. After that a temperature log was again taken.

The conductivity logs are shown in Figures 16 and 17. Figure 16 shows only the upper portion of the section studied (700-1000 m), displaying two inflow points; Figure 17 shows the full section displaying nine major inflow points. For the sake of discussion, these peaks are labeled 1 through 9, as shown in these figures. The wellbore diameter over the

section is 5 1/2 inches or 14 cm. The temperature log shows an increase of temperature with depth that can be approximated adequately by

$$T = 10 + \frac{x}{30} \tag{11}$$

where x is in meters and T in °C. The fluid electric conductivity, $\sigma$, depends on temperature. In order to convert the measured values shown in Figures 16 and 17 to normalized conductivity values at a uniform temperature, $T_n$, of 20°C, the following formula (NAGRA, 1987) is used:

$$\sigma\,(T_n) = \frac{\sigma(T)}{1 + 0.022\,(T-20)} \tag{12}$$

The field data are digitized and then normalized according to equations (11) and (12). The normalized electric conductivity log is shown in Figure 18. Now we proceed to study and match the nine peaks in this figure.

First let us calculate the Reynold's number, R, for flow in this case. By equation (1) we see $R = vd/\nu$. For well head pumping rate Q = 20 *l*/min, wellbore diameter is d = 14 cm, and $\nu$ is given by water kinematic viscosities at the appropriate temperatures ($0.3 - 1 \times 10^{-6}$ $m^2/s$), the Reynold's number at the well head is $R \approx 3000$. This is above the critical value and the flow is in the laminar-turbulent transition region. If Q = 2 *l*/min, then $R \approx 300$, much smaller than the critical Reynolds number of 2000.

The positions of the nine peaks range from the deepest one (peak 1) at x = 1440 m to the most shallow one (peak 9) at x = 843 m. We have selected an arbitrary starting time of pumping as a reference. Peaks 8 and 9 have data at 13.03 hours relative to this reference time. All peaks have data at 27.12, 31.28, 38.41 and 57.24 hours. We consider the starting times of these inflows to be unknown and possibly different from each other. First let us treat these peaks independently and apply the results from equations (5) - (7), where we convert the concentration C to conductivity values $\sigma$ by means of equation (1).

Figure 19 shows the plots of $[\sigma(0,t)]^2$ versus time t. We assume that only the data at the earliest two to three times satisfy the early time requirements of equation (5). Then a line joining these early time values yields the slope and intercept, which corresponds to $S_c = 16(\alpha q C_o)^2/\pi^3 D d^4$ and $t_o$ for each peak respectively. These values

are listed in Table 1. Figure 20 shows the plot of $\int \sigma(x,t)dx$ versus time t. Again, the slopes and intercepts of the early times are found and listed in Table 2. It is noted that the $t_o$ values found for each peak from these two methods do not agree with each other. This may be due to numerical difficulties in determining the peak value and the area under each of the curves and the assumptions underlying equation (5). For the case of peak 9, the data are incomplete at the lower x values and, for peak 4, the $\sigma(0,t)$ value is hard to determine because of the overlap of neighboring curves. An interesting result is the ratio, $S_A^2/S_c$, of the slopes obtained for each peak. As explained in an earlier section, this should be equal to $\pi D$, a constant for all the peaks. The results of Table 2 show that, omitting peak-4 and peak-9 data, the values are within a factor of two of each other, with a mean value of $\overline{\pi D} = 24.8$ m$^2$/hr or $7 \times 10^{-3}$ m$^2$/s. This is much larger than would be expected for molecular diffusion which typically yields a value for $D_m \approx 10^{-8}$ m$^2$/s. The larger value for $\overline{\pi D}$ in our problem, we believe, is due to dilution effect during the initial inflow of high-salinity water into the borehole cross-section of finite radius. If the borehole radius were zero or negligible, diffusion would just occur along the length of the well, which is the case described by our early-time analytic solution. Since the borehole has finite radius, the dilution of incoming saline water within the cross-section results in a large effective diffusion coefficient. For advection-dispersion calculations of saline water up the wellbore, the smaller $D_m$ value may be the more appropriate one to use.

Having made the above analysis, we proceed to apply the numerical code described in the last section to match all nine peaks and attempt to obtain the parameters $t_{oi}$, $q_i$ and $C_{oi}$. First we need initial guesses for these parameters, which are obtained as follows. For each peak, we can easily determine its location, $x_i$, by inspection of Figure 18. The quantity $q_i C_{oi}$ can be obtained in two ways. The first is to use the value of $S_c$ from Table 1 and the mean value of $\overline{\pi D}$ to calculate:

$$q_i C_{oi} = \sqrt{S_c(\overline{\pi D})} \cdot (\pi d^2/4)/\alpha \qquad (13)$$

The other way is to use $S_A$ from Table 2 directly and solve for $q_i C_{oi}$ by:

$$S_A = 4\alpha q_i C_{oi}/\pi d^2 \qquad (14)$$

In principle, the values of the parameters, $t_{oi}$ and $q_i C_{oi}$, obtained from Tables 1 and 2 should be the same if the early time requirement is satisfied. The present data set does not give equal parameter values, because insufficient data were obtained in the first 10-15 hours. The uncertainties are particularly large for the highest two peaks, peaks 9

and 8, which carry most of the flow. Also, the borehole diameter, d, may not be constant along the length of the borehole. Hence, in choosing the parameter values we have considered both Table 1 and Table 2 in a complementary way and have come up with a set of initial guesses. Then, these are adjusted to obtain parameters for the numerical code that yield the best match to observed data.

The primary parameter to be determined is $q_i$, the value of the flow rate for each inflow point. Since we do not have data corresponding to large-time limit data in order to use equations (1) - (3), these have to be found by successive guesses, under the constraint that

$$\Sigma q_i = Q,$$

if Q can be measured independently. For the present data set, the value of Q is uncertain (see below).

The wellbore dispersivity parameter, K, is given by equation (9), where d = 14 cm, and q and D will be estimated as follows. Anticipating the results of data-matching discussed below, q for the whole section of the borehole under study (≈770 - 1637 m) is about 2 *l*/min. However the highest two inflow points at 843 m and 918 m represent 80% of the total flow. So the approximate mean flow rate over the remainder of the borehole section is assumed to be 0.2 *l*/min. Based on the discussions above, we decide that it is inappropriate to use a value of D derived from $\overline{\pi D} = 7 \times 10^{-3}$ m$^2$/s, because of the borehole cross-section dilution effect. Instead, we assume that $D = D_m \approx 10^{-8}$ m$^2$/s. Using these parameters, we find that $K = 5 \times 10^{-4}$ m$^2$/s. This is used as the initial guess value. Slight adjustment can then be made on K to optimize the data match.

A number of attempts of data matching are made, some of which are shown below. Table 3 shows the parameters for one of our first attempts. In this table, $q_i C_{oi}$ are obtained using equation (14). The values of $q_i$ are assumed to be proportional to $q_i C_{oi}$ and, based on earlier information we received should add up to $Q = 3.3 \times 10^{-4}$ m$^3$/s (≈20 *l*/min). The results are shown in Figure 21. It is apparent from this figure that all the peaks are much lower than the observed data (Figure 18). A few further attempts show us that it is impossible to match the data with this assumed value of Q. By adjusting Q, we found that we can match the data if Q ≈ 2 *l*/min, ten times less than the number we used originally. We then sent a request to NAGRA (1987), who went back to the field data and found that the value of flow rate from the field experiment may be dominated by flow from a wellbore section above the section under study. The value of Q may indeed be only $3.3 \times 10^{-5}$ m$^3$/s or 2 *l*/min. This is used for all

later calculations.

Table 4 gives the parameters for the base case used for the sensitivity studies. These are the same as Table 3 except all the $q_i$ values are reduced by a factor of 2 and hence $C_{oi}$ values are increased by a factor of 2 in order to keep $q_iC_{oi}$ constant. The results are shown in Figure 22. Now the key parameters are varied to display the sensitivity of the peaks to these variations. Figure 23 shows the results when the dispersion coefficient is changed from $5 \times 10^{-4}$ $m^2/s$ to $5 \times 10^{-5}$ $m^2/s$. The results are relatively insensitive. Figure 24 shows the results based on parameters given in Table 4 except that $q_i$ are all reduced by as factor of 2, and $C_{oi}$ increased by a factor of 2, while keeping $q_iC_{oi}$ constant. Figure 25 shows the results based on parameters given in Table 4 except that $q_i$ are increased by a factor of 2 and $C_{oi}$ are decreased by a factor of 2, while keeping $q_iC_{oi}$ constant. The dependence on these variations are quite instructive. The next two sets of calculations are made by reducing all $q_iC_{oi}$ by a factor of 2 relative to the base case. This may be done by either decreasing $q_i$ by a factor of 2, or by decreasing $C_{oi}$ by a factor of 2, with the results displayed in Figures 26 and 27 respectively.

After these sensitivity studies, the parameters for each peak are varied to obtain a best fit to observed data (Figure 18). The best fit was obtained by visually comparing calculated and observed curves. The results are shown in Figures 28 with the final matching parameters listed in Table 5. Figure 29 displays both the matching results and the observed data for the time = 57.24 hrs.

We next extrapolate the results to future times assuming the parameters in Table 5. The results shown in Figure 30 are the predicted results if the experiment were to be continued for a longer period of time.

## 6 CONCLUSION AND DISCUSSION

In this paper we first discussed the procedure and physical processes associated with a time series of fluid conductivity logs in a borehole intersected by a number of flowing fractures. Simple formulas to evaluate some of the relevant parameters are described and their uses demonstrated. Then numerical matching of the data to obtain the remaining parameters is shown. The results are not sensitive to borehole radius variations and the method may be able to measure small inflow rates. From Table 4, it appears that flow rate as low as 0.2 x $10^{-6}m^3/s$ or 0.01 *l*/min can be measured. This may prove to be a useful technique and may complement existing flow-meter or temperature-log methods.

To conclude this paper, we will briefly discuss some practical aspects as

well as some of the limitations and advantages of the proposed borehole fluid electric-conductivity logging method.

Obviously for a successful test it is necessary to create inflow from the formation into the borehole, which requires the lowering of the pressure in the borehole fluid column below the formation pressure. Water from the borehole could be swabbed or intermittently pumped, although the analysis can be easier if constant rate pumping is conducted. Further, a significant contrast in electric conductivity between the formation water and the borehole fluid is required. In the case of high conductivity of the formation water a low conductivity fluid should be applied in the borehole and vice versa.

As any experimental technique, electric conductivity logging is subject to detection limits. The lower detection limit for inflowing formation water is determined by the ability to properly identify and quantify electric conductivity changes caused by the inflow. This is controlled by processes which dissipate the electric conductivity contrast between the formation water and the borehole fluid. Two processes are important: (i) dispersion in the borehole, which tends to smear out the electric conductivity peaks; and (ii) dilution of the inflowing formation water by the existing flow within the borehole, which limits the maximum conductivity values of these peaks. In Leuggern borehole it was possible to detect and quantify single inflows down to some 5 to 10 ml/min corresponding to fracture transmissivities as low as $10^{-9}$ to $10^{-10}$ $m^2/s$. It is the dilution of the water flowing in the borehole that causes the most severe limitation. Because the inflow is a fraction of the flow in the borehole, the detection limit increases towards the pump, since the flow rate in the borehole, being the sum of all the inflows, also increases towards the pump. However, dilution can be controlled to some extent by isolating, for example with a packer, a higher producing part of the borehole and testing the remaining section above it. This procedure was successfully applied in the Leuggern borehole.

An upper detection limit is created by high flows in the borehole. In this case, the borehole fluid is replaced by formation water at a speed which is too fast for properly logging the growth rate of the peaks. This is indicated in Leuggern borehole near the top of the logged section, where conductivity saturation was reached already before the first logging run took place. Maximum flow rates in the borehole can to some extent be controlled by adjusting the pump rate. However, in case of large differences in the formation head along the borehole, natural flow without pumping might be too high. If this is the case, application of a borehole spinner flowmeter seems more appropriate.

Based on the experience NAGRA gained during the conduction of the feasibility studies and safety analyses for Project Gewhr 1985, which

involved an extensive regional investigation program in deep boreholes drilled in sedimentary-covered crystalline rocks in Northern Switzerland (Nagra, 1985; Thury and Gautschi, 1986; Nagra, 1988), fluid-logging techniques have several advantages. First, they allow an identification of the locations of water-conducting fractures or groups of fractures in a borehole. This is very important for subsequent core investigations aiming at a detailed geological and geochemical description of preferential flow paths and its surrounding rock. Secondly, fluid-logging may be used to derive the hydraulic or flow properties, like transmissivity, of these identified water-conducting features. Such a technique would be a cost effective alternative to the conventional hydraulic single and double packer testing. Even if conventional hydraulic testing would not be completely dismissed, fluid logging could effectively be applied as a screening tool prior to a subsequent hydraulic testing and water sampling program. In conclusion, even though there are limitations to the proposed method, the advantages discussed above render the method quite promising.

Future work will be directed towards expanding the method to generate the transmissivity distribution along the borehole. This will require the coupling of the model which calculates the transport in the borehole with a code that calculates the inflow from the formation based on the formation hydraulic properties. The required pressure distribution in the borehole would be calculated from another code where the effects of the temperature and salinity distribution, measured during the logging, on fluid pressure could be also taken into consideration.

## 7 ACKNOWLEDGEMENTS

Discussions and cooperation with NAGRA personnel, especially M. Thury, A. Zingg, and P. Zuidema are much appreciated. Assistance in computation and graphing from C. Doughty and F. Hale are gratefully acknowledged. We would also like to thank C. Doughty, N. Goldstein, and I. Javandel for reviewing and commenting on the manuscript. The work is jointly supported by Nationale Genossenschaft für die Lagerung radioaktiver Abfälle, Switzerland; Engineering and Geoscience Division, Office of Basic Energy Sciences; and Repository Technology Division, Office of Civilian Radioactive Waste Management, U. S. Department of Energy through Contract No. DE-AC03-76SF00098.

## REFERENCES

Aris, R. (1956), On the dispersion of a solute in a fluid flowing through a tube, *Proc. R. Soc. London,* Series A 235, 67-77.

Bean, H. S. (1971), *Fluid meters: Their theory and application,* American Association of Mechanical Engineers, 6th Edition, New York.

Bodvarsson, G. S. (1982), Mathematical modeling of the behavior of geothermal systems under exploitation, Ph.D. Thesis, University of California at Berkeley, Department of Materials Sciences and Mineral Engineering.

Fischer, H. B., E. J. List, R. C. Y. Koh, J. Imberger, N. H. Brooks (1979), *Mixing in Inland and Coastal Waters,* Academic Press, New York.

Hale, F. V. and C. F. Tsang, (1988): *A Code to Compute Borehole Fluid Conductivity Profiles with Multiple Feed Points,* NAGRA Technical Report NTB 88-21, Nagra, Baden, Switzerland.

Hufschmied, P. (1983), Ermittlung der Durchlässigkeit von Lockergesteins - Grundwasserleitern, eine vergleichende Untersuchung verschiedener Feldmethoden, Diss. No. 7397, ETH Zurich, Switzerland.

Javandel, I., C. Doughty and C. F. Tsang (1984), *Groundwater Transport,* Water Resources Monograph No. 10, American Geophysical Union, Washington, D. C.

NAGRA (1985), Project Gewähr 1985, Nuclear Waste Management in Switzerland: Feasibility Studies and Safety Analyses, NAGRA Project Report NGB 85-09, Nagra, Baden, Switzerland, June 1985.

NAGRA (1987), Private Communication, NAGRA, Baden, Switzerland.

NAGRA (1988), Fluid-Logging der Sondierbohrungen Böttstein, Weiach, Riniken, Schafisheim, Kaisten and Leuggern, Temperature-, Leitfahigkeits- und Spinner flowmeter-Messungen, NAGRA Technical Report NTB 85-10, Nagra, Baden, Switzerland, in preparation.

Ogata, A. and R. B. Banks (1961), A solution of the differential equation of longitudinal dispersion in porous media, U. S. Geological Survey Prof. Pap. 411A, 34 pp.

Omega (1987), *Complete Flow and Level Measurement Handbook and Encyclopedia,* Omega Engineering, Inc., Stamford, Connecticut.

Roberson, J. A. and C. T. Crowe (1985), *Engineering Fluid Mechanics,* Houghton Mifflin Publishing Company, Boston, Massachusetts.

Shedlovsky, T., and L. Shedlovsky (1971), "Conductometry," *Techniques of Chemistry,* (Arnold Weissberger and Bryant W. Rossiter, eds.), Vol. 1. Physical Methods of Chemistry, Part IIa, Electrochemical Methods, John Wiley & Sons, Inc., New York.

Taylor, G. I. (1953), Dispersion of solute matter in solvent flowing slowly through a tube, *Proc. R. Soc. London,* Series A 219, 186-203.

Thury, M., and A. Gautschi (1986), Testing programme in deep boreholes drilled in sediment-covered crystalline rocks in northern Switzerland, *Proceedings of the 2nd International Conference on Radioactive Waste Management,* September 7-11, 1986, Winnipeg, Manitoba, Canada.

Tsang, C. F. (1985), Lessons learned in the verification and validation studies of a coupled heat and fluid flow code, Invited Paper, Proceedings of Symposium on Groundwater Flow and Transport Modeling for Performance Assessment of Deep Geologic Disposal of Radioactive Waste: A Critical Evaluation of the State of the Art, May 20-21, 1985, Albuquerque, New Mexico.

Tsang, C. F. and C. Doughty (1985), Detailed validation of a liquid and heat flow code against field performance, Proceedings of the Eighth SPE Symposium on Reservoir Simulation, February 10-13, 1985, Dallas, Texas, organized by Society of Petroleum Engineers, Richardson, Texas.

Table 1: Data from $[\sigma(0,t)]^2$ vs t curves.

| Peak No. | x (meters) | $t_{oi}$ (hours) | $S_c$ $(\mu S)^2/cm^2hr$ |
|---|---|---|---|
| 1 | 1440 | 18 | 929 |
| 2 | 1300 | 16 | 339 |
| 3 | 1215 | 19 | 711 |
| 4 | 1200 | 21 | (854) |
| 5 | 1188 | 19 | 892 |
| 6 | 1085 | 17 | 73 |
| 7 | 1048 | 2 | 402 |
| 8 | 918 | 9 | 55663 |
| 9 | 843 | -24 | 34310 |

Table 2: Data from $\int_{-\infty}^{\infty} \sigma(x,t)\, dx$ vs t curves.

| Peak No. | x (meters) | $t_{oi}$ (hours) | $S_A$ (100 $\mu$S/hr) | $S_A^2/S_c$ ($m^2$/hr) |
|---|---|---|---|---|
| 1 | 1440 | 6 | 145 | 22.6 |
| 2 | 1300 | 3 | 102 | 30.7 |
| 3 | 1215 | 11 | 111 | 17.3 |
| 4 | 1200 | 13 | 47 | (2.59) |
| 5 | 1188 | 13 | 121 | 16.4 |
| 6 | 1085 | 11 | 40 | 21.9 |
| 7 | 1048 | 8 | 118 | 34.6 |
| 8 | 918 | 6 | 1243 | 27.8 |
| 9 | 843 | 6 | (5449) | (866) |

Table 3: Parameters used in initial match of field data

| Peak No. | x (meters) | $t_{oi}$ (hours) | $q_iC_{oi}$ ($10^{-6}$kg/s) | $q_i$ ($10^{-6}$ $m^3$/s) | $C_{oi}$ (kg/$m^3$) |
|---|---|---|---|---|---|
| 1 | 1440 | 18 | 0.33 | 6.5 | 0.051 |
| 2 | 1300 | 18 | 0.23 | 4.6 | 0.051 |
| 3 | 1215 | 18 | 0.26 | 5.0 | 0.051 |
| 4 | 1200 | 18 | 0.11 | 2.1 | 0.051 |
| 5 | 1188 | 18 | 0.28 | 5.4 | 0.051 |
| 6 | 1085 | 18 | 0.09 | 1.8 | 0.051 |
| 7 | 1048 | 2 | 0.27 | 5.3 | 0.051 |
| 8 | 918 | 9 | 2.9 | 56 | 0.051 |
| 9 | 843 | -24 | 13 | 240 | 0.051 |
| $K = 5.0 \times 10^{-4}$ $m^2/s$<br>$Q = 3.3 \times 10^{-4}$ $m^3/s$ | | | | | |

Table 4: Parameters used in sensitivity analysis: Base Case

| Peak No. | x (meters) | $t_{oi}$ (hours) | $q_iC_{oi}$ ($10^{-6}$ kg/s) | $q_i$ ($10^{-6}$ $m^3$/s) | $C_{oi}$ (kg/$m^3$) |
|---|---|---|---|---|---|
| 1 | 1440 | 18 | 0.33 | 0.65 | 0.51 |
| 2 | 1300 | 18 | 0.23 | 0.46 | 0.51 |
| 3 | 1215 | 18 | 0.26 | 0.50 | 0.51 |
| 4 | 1200 | 18 | 0.11 | 0.21 | 0.51 |
| 5 | 1188 | 18 | 0.28 | 0.54 | 0.51 |
| 6 | 1085 | 18 | 0.09 | 0.18 | 0.51 |
| 7 | 1048 | 2 | 0.27 | 0.53 | 0.51 |
| 8 | 918 | 9 | 2.9 | 5.6 | 0.51 |
| 9 | 843 | -24 | 13. | 24. | 0.51 |
| $K = 5.0 \times 10^{-4}$ $m^2/s$<br>$Q = 3.3 \times 10^{-5}$ $m^3/s$ | | | | | |

Table 5: Parameters used in final match of field data.

| Peak No. | x (meters) | $t_{oi}$ (hours) | $q_iC_{oi}$ ($10^{-6}$kg/s) | $q_i$ ($10^{-6}$ $m^3$/s) | $C_{oi}$ (kg/$m^3$) |
|---|---|---|---|---|---|
| 1 | 1440 | 18 | 0.23 | 0.65 | 0.35 |
| 2 | 1300 | 18 | 0.09 | 0.46 | 0.20 |
| 3 | 1215 | 18 | 0.23 | 0.50 | 0.45 |
| 4 | 1200 | 18 | 0.09 | 0.21 | 0.45 |
| 5 | 1188 | 18 | 0.24 | 0.54 | 0.45 |
| 6 | 1085 | 18 | 0.06 | 0.18 | 0.35 |
| 7 | 1048 | 2 | 0.27 | 0.53 | 0.50 |
| 8 | 918 | 9 | 4.2 | 1.5 | 2.80 |
| 9 | 843 | -24 | 25. | 28. | 0.90 |
| $K = 5.0 \times 10^{-4}$ $m^2/s$<br>$Q = 3.3 \times 10^{-5}$ $m^3/s$ | | | | | |

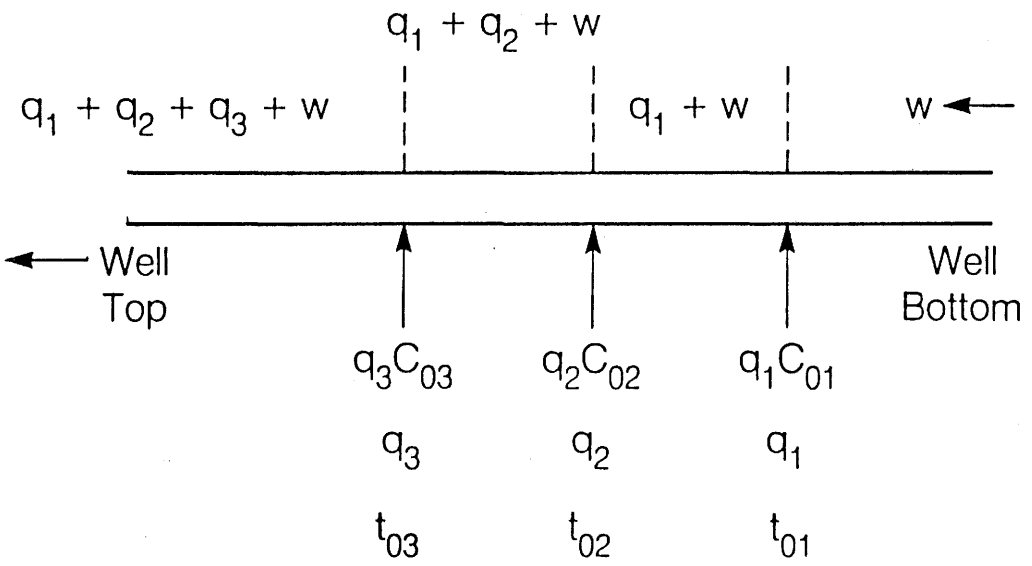


Figure 1: Schematic picture of a wellbore with three inflow points and a well-bore rate w from below.

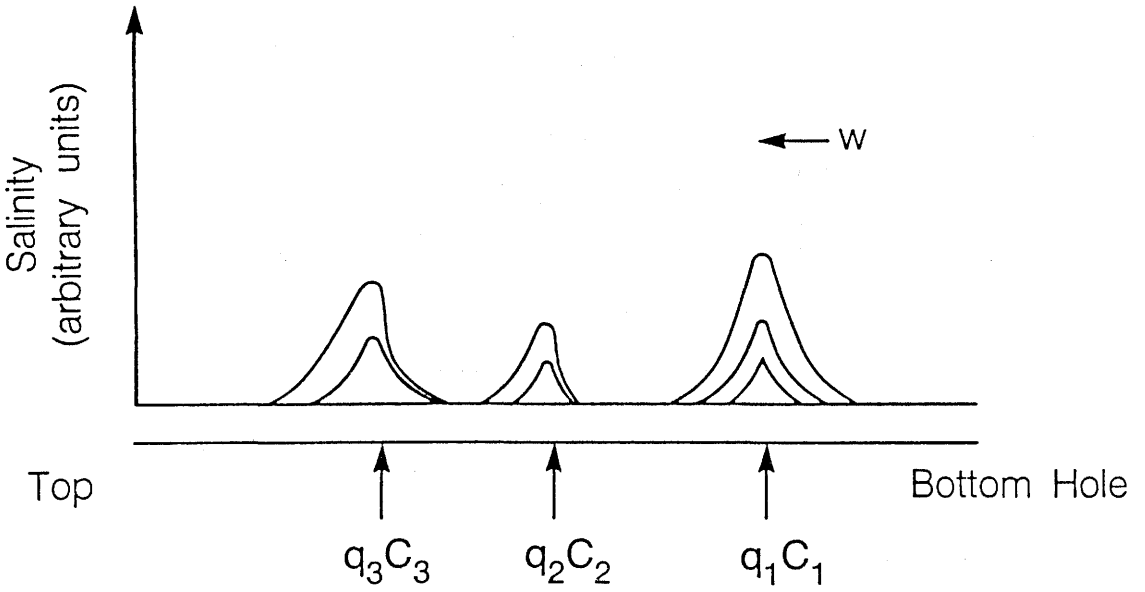


Figure 2: Schematic picture of salinity curves from three inflow points in a wellbore at early times.

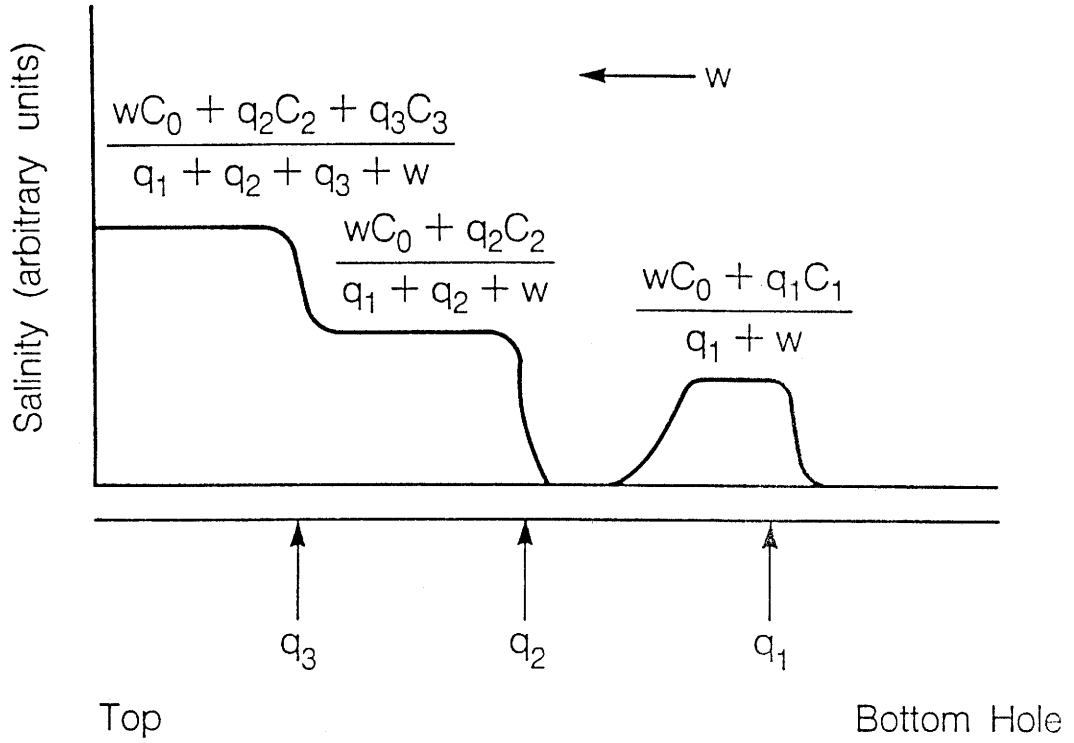


Figure 3: Schematic picture of salinity curves at a large time, assuming very small diffusion effects.

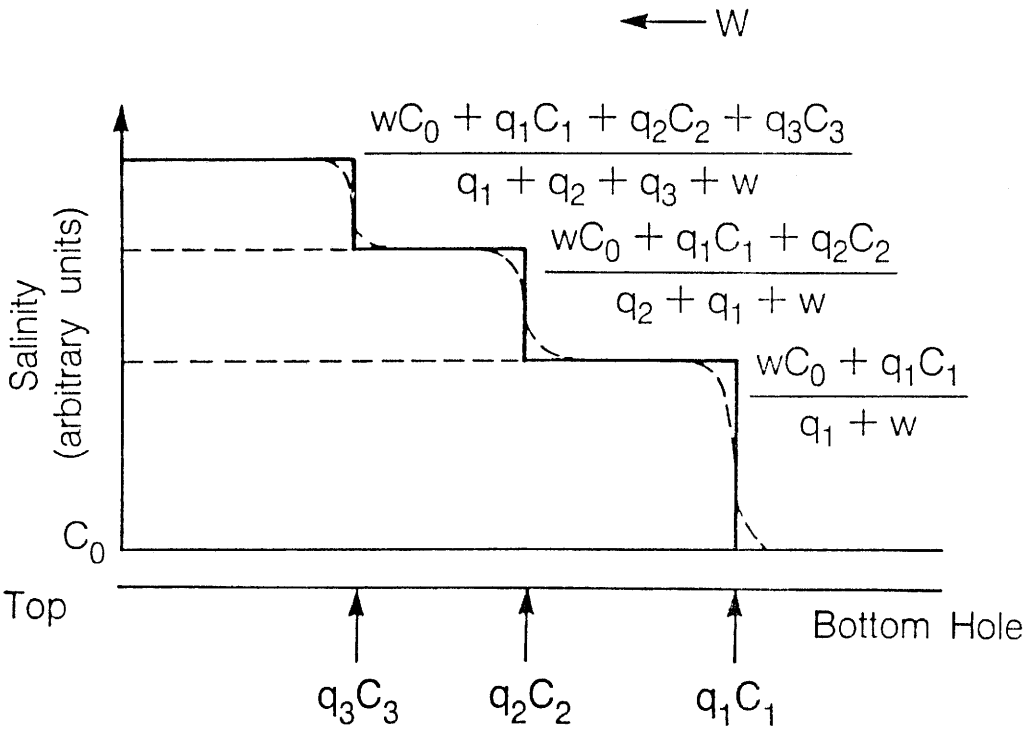


Figure 4: Schematic picture of salinity concentration curves at the very large time limit, assuming very small diffusivity effects.

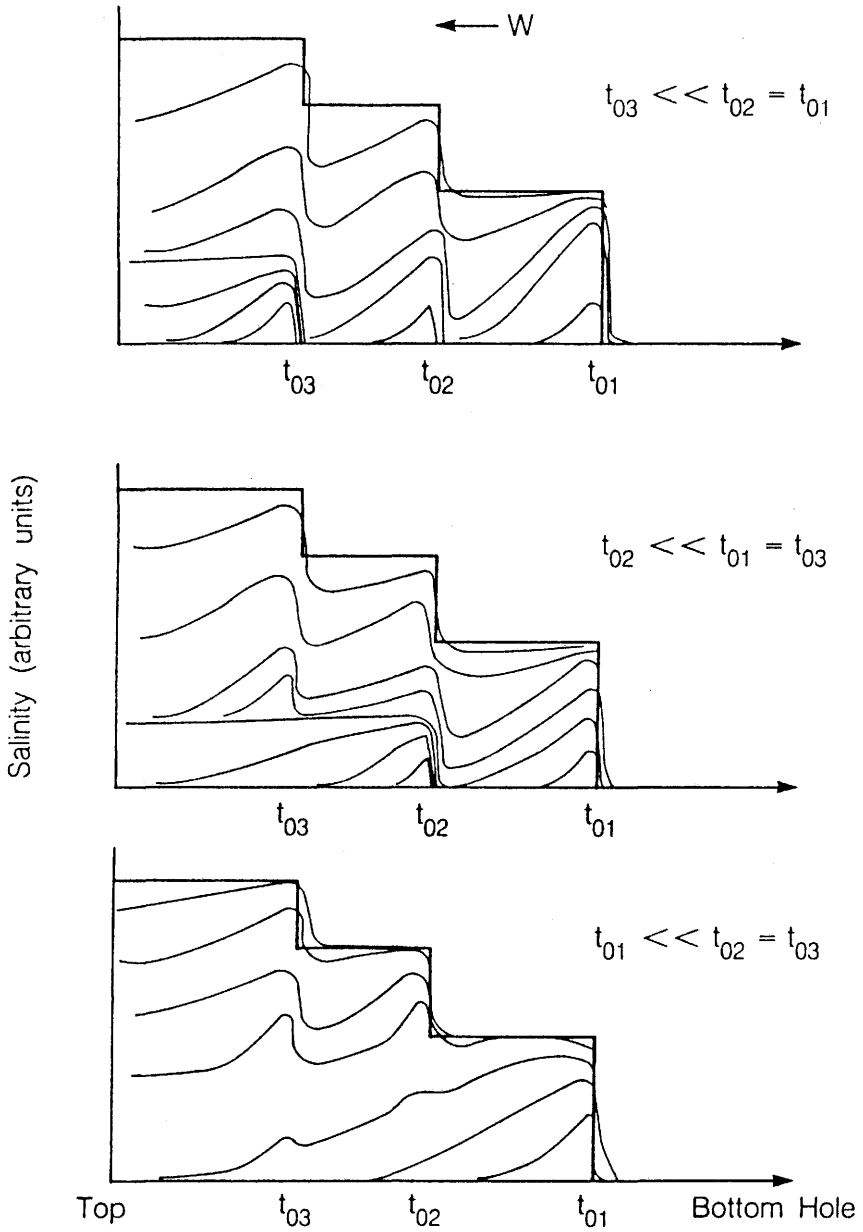


Figure 5: Schematic picture of salinity concentration curves from early to later times, assuming one of the three inflow points begins much earlier than the other two.

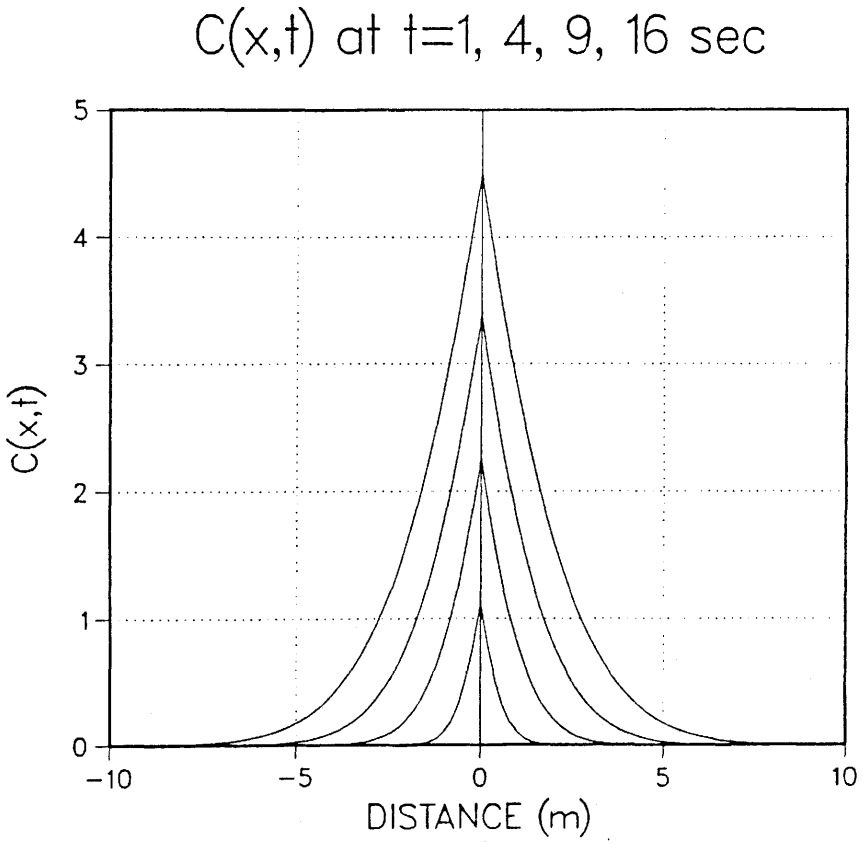


Figure 6: Analytic results for one inflow point for early times.

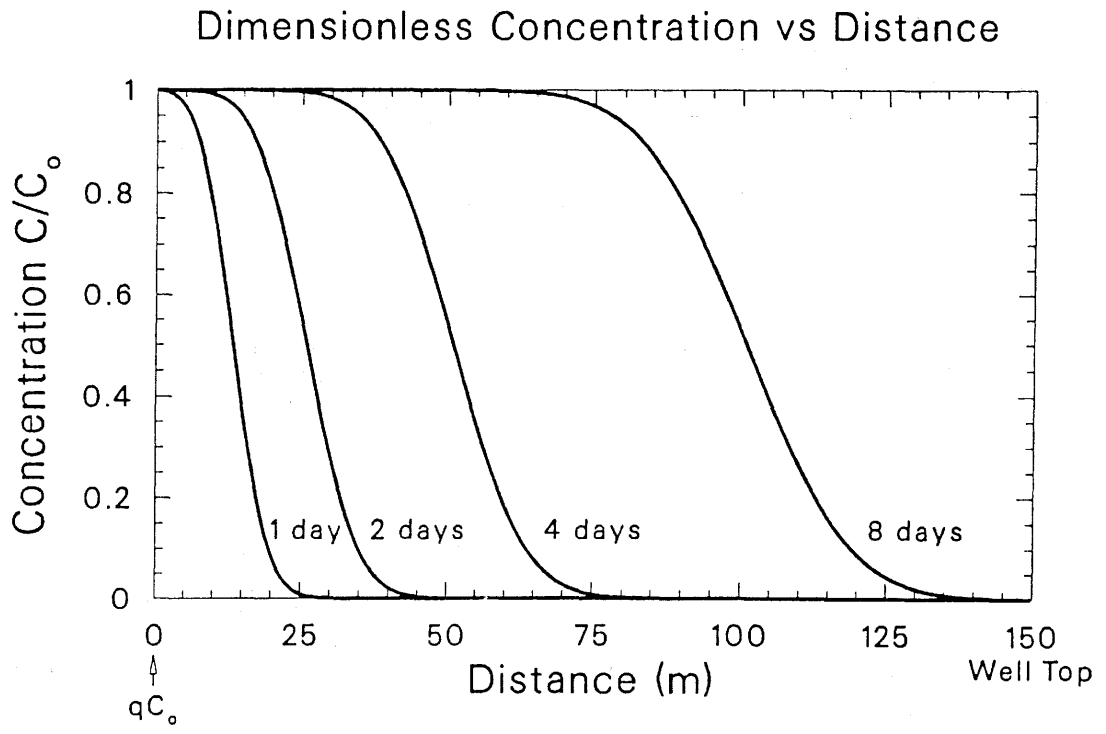


Figure 7: Analytic results for one inflow point for later times.

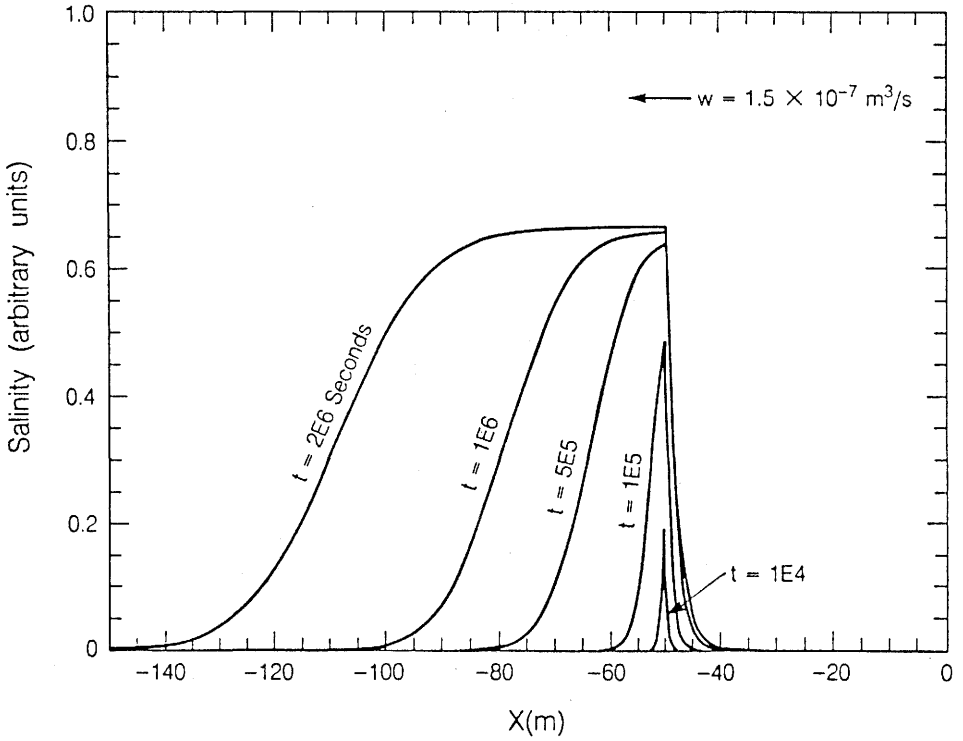


Figure 8: Numerical results for one inflow point from early to later times.

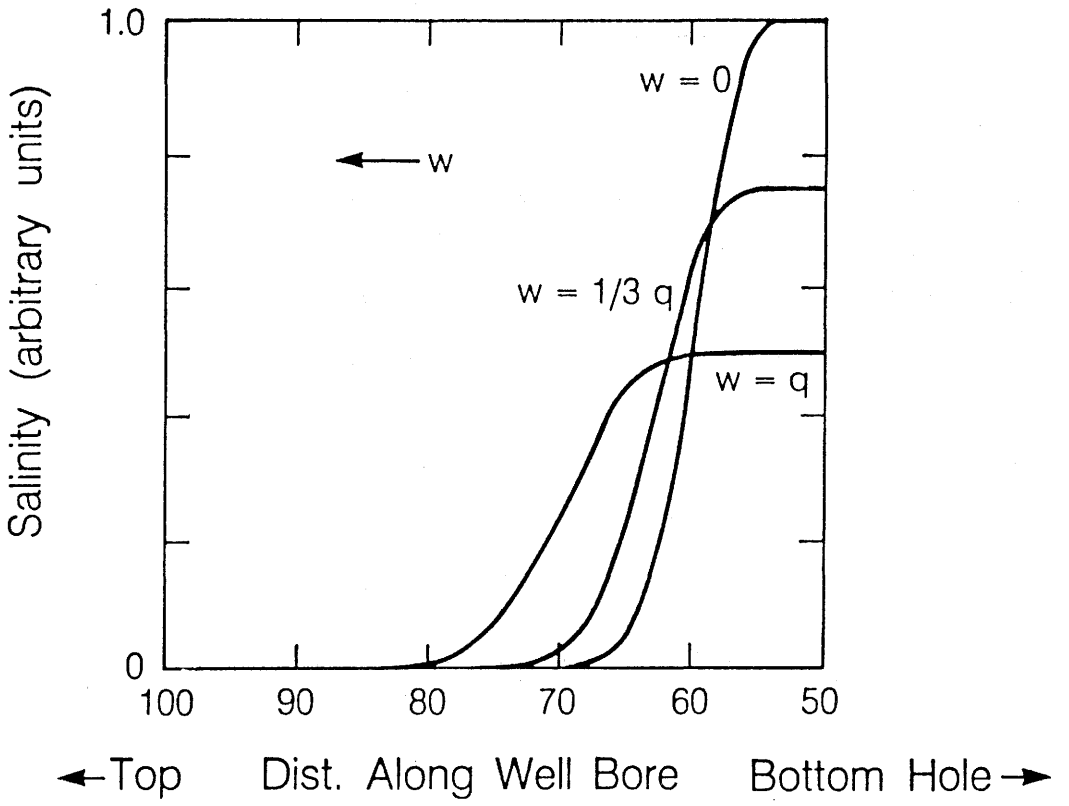


Figure 9: Numerical results for one inflow point at flowrate q for three values of wellbore flow rate from below: w = 0, w= q/3 and w = q.

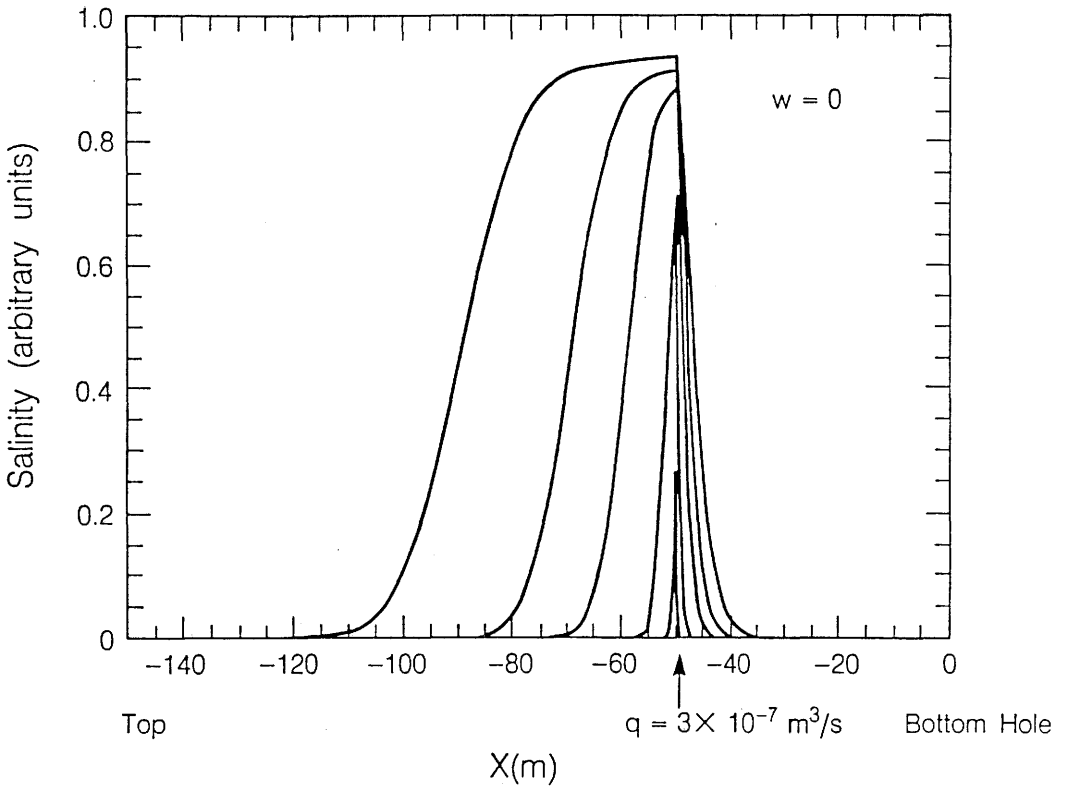


Figure 10a: Numerical results for one inflow point and w = 0 for dispersion constant K equal to 25 m²/s.

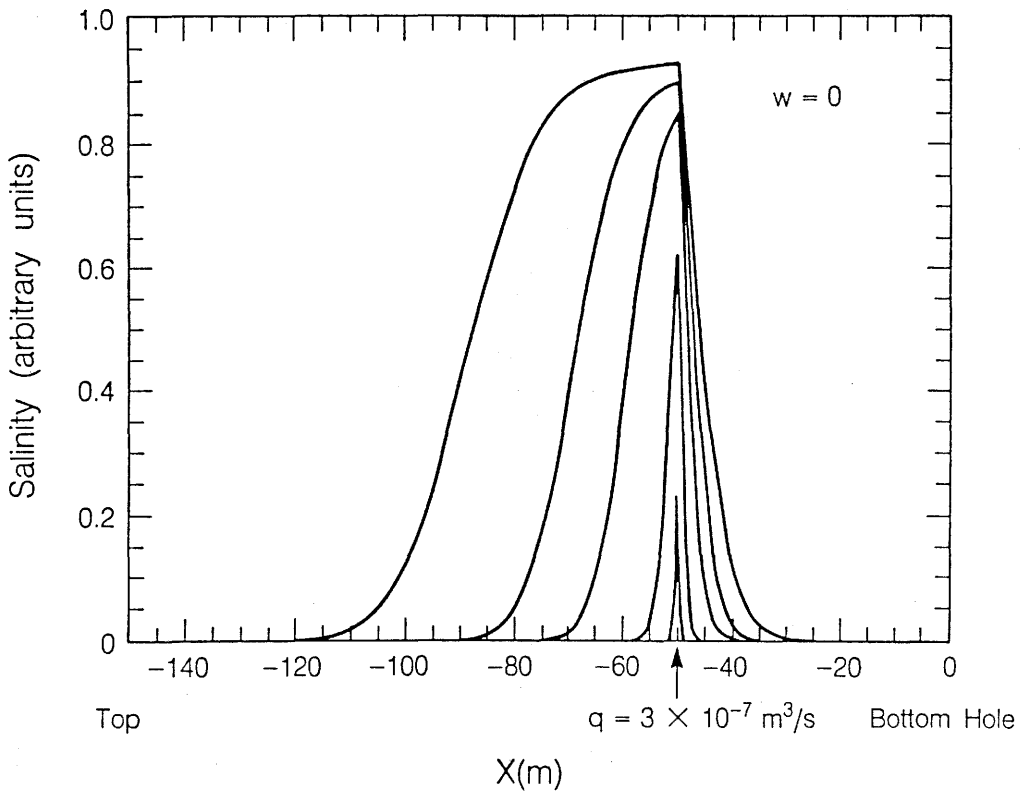


Figure 10b: Numerical results for one inflow point and w = 0 for dispersion constant K equal to 50 m²/s.

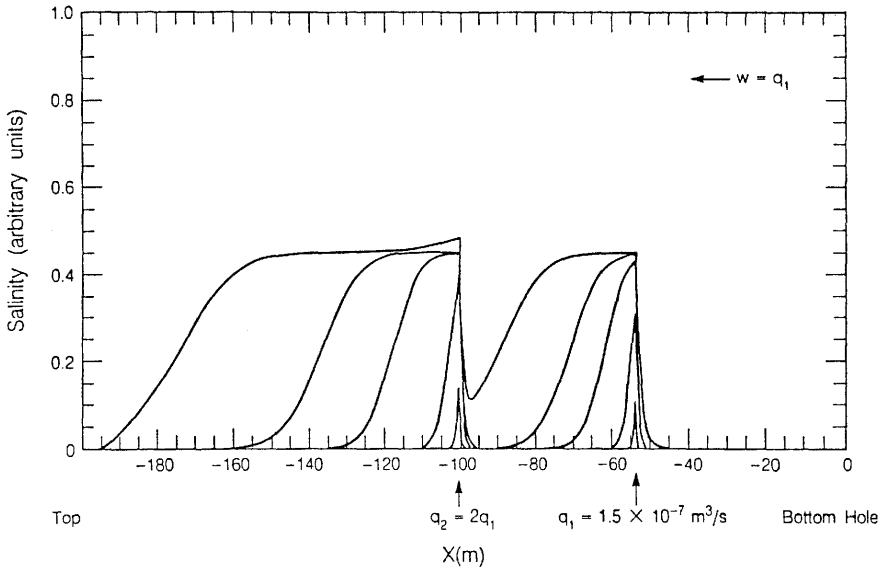


Figure 11: Numerical results for two inflow points.

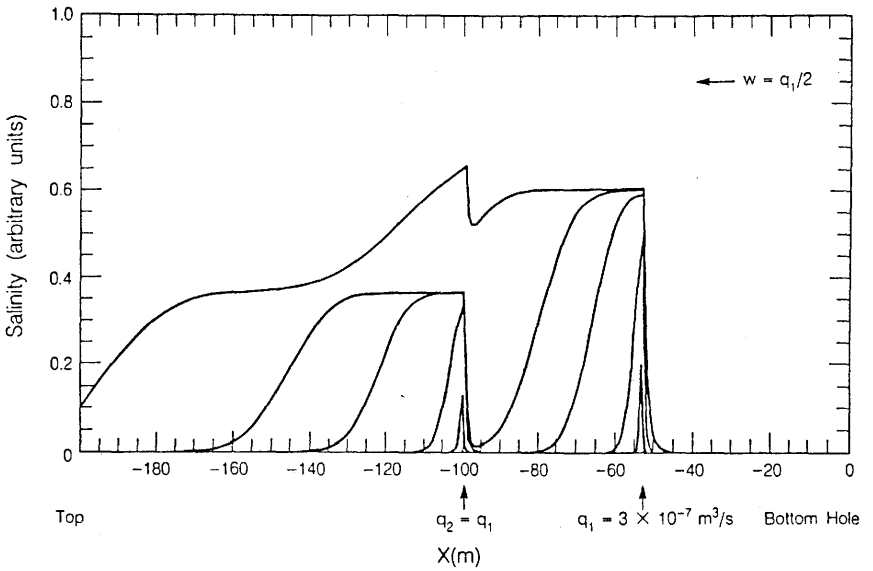


Figure 12: Numerical results for two points, displaying interference.

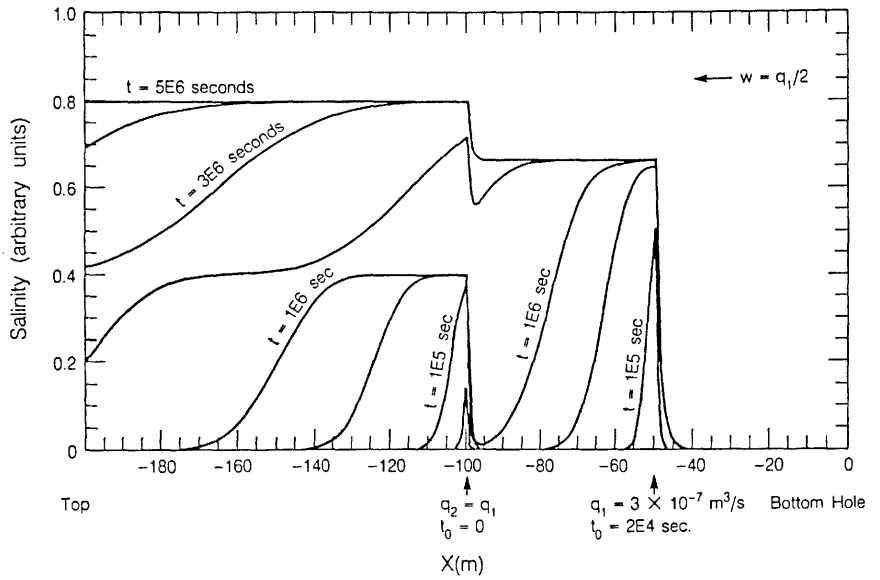


Figure 13: Numerical results for two inflow points for large time limit.

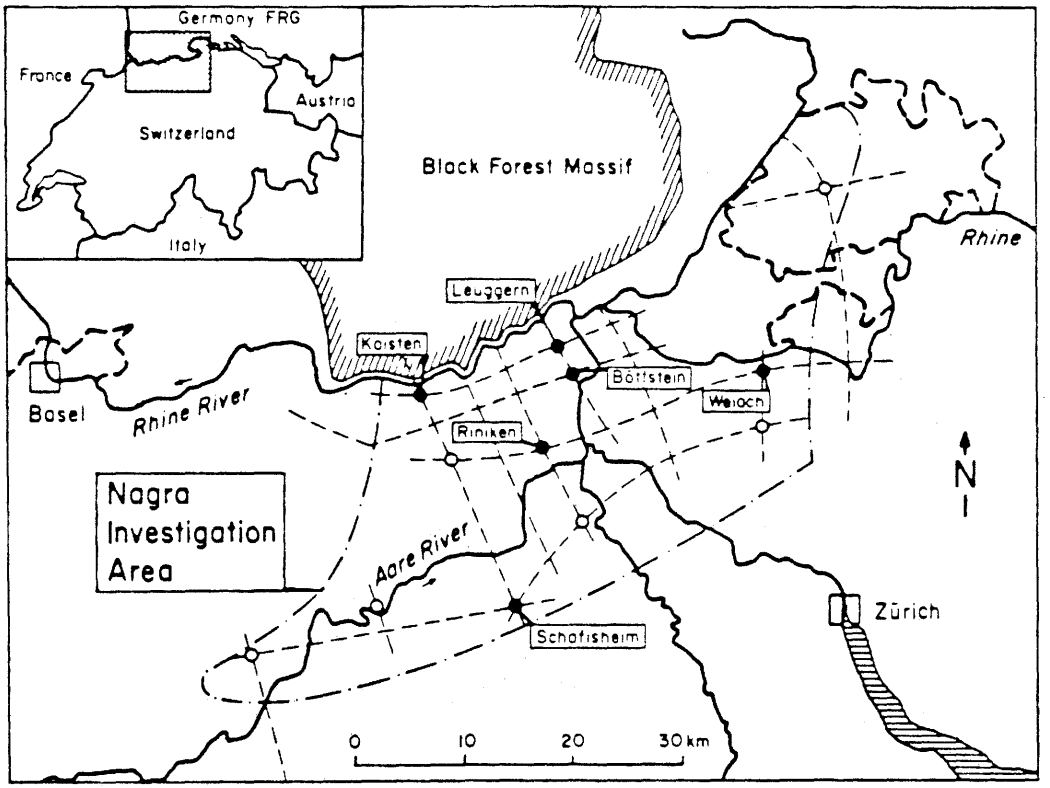


Figure 14: Map of Northern Switzerland, with the location of the Leuggern borehole.

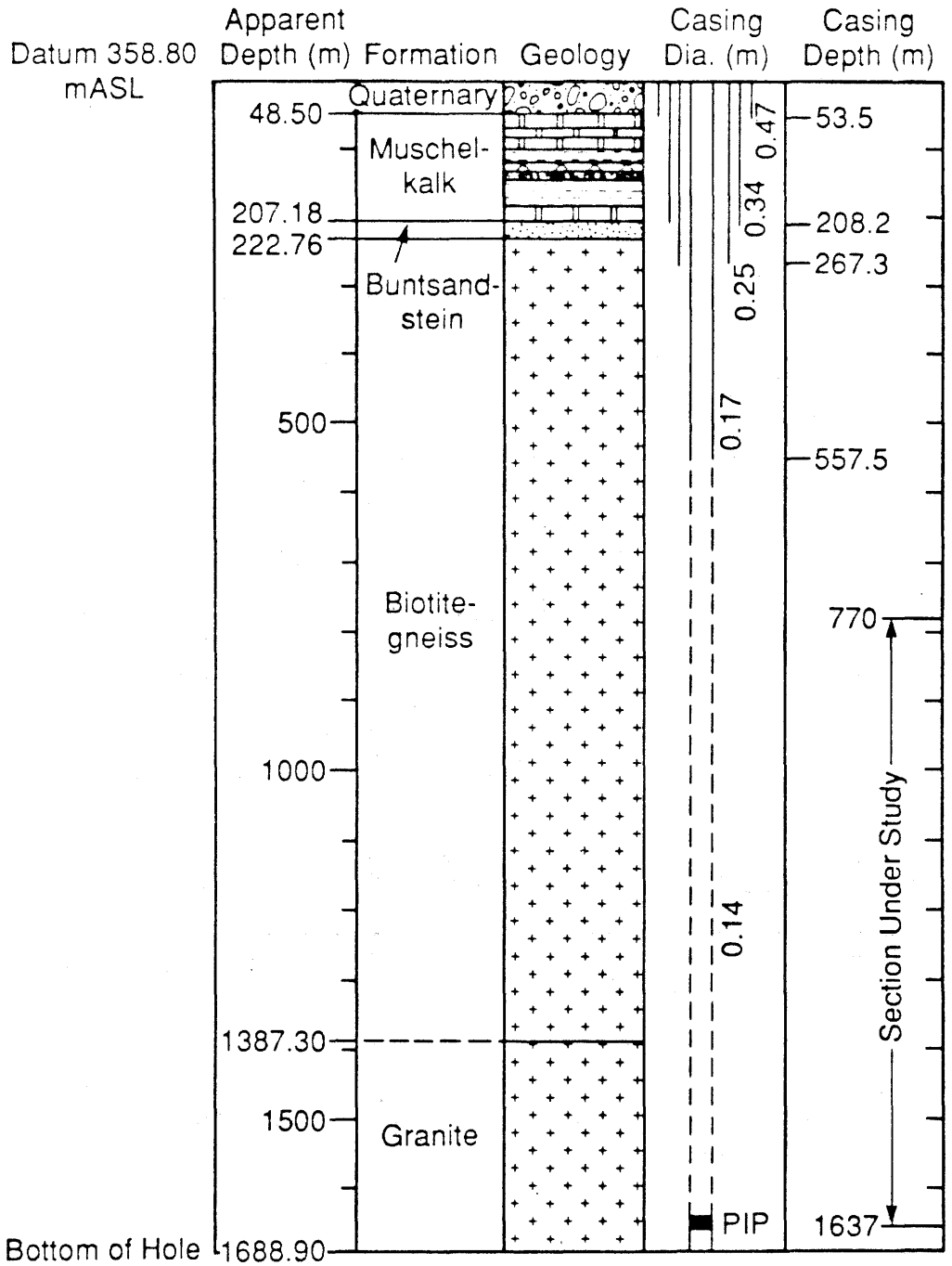


Figure 15: Geological formations intersected by the Leuggern borehole, and other borehole characteristics.

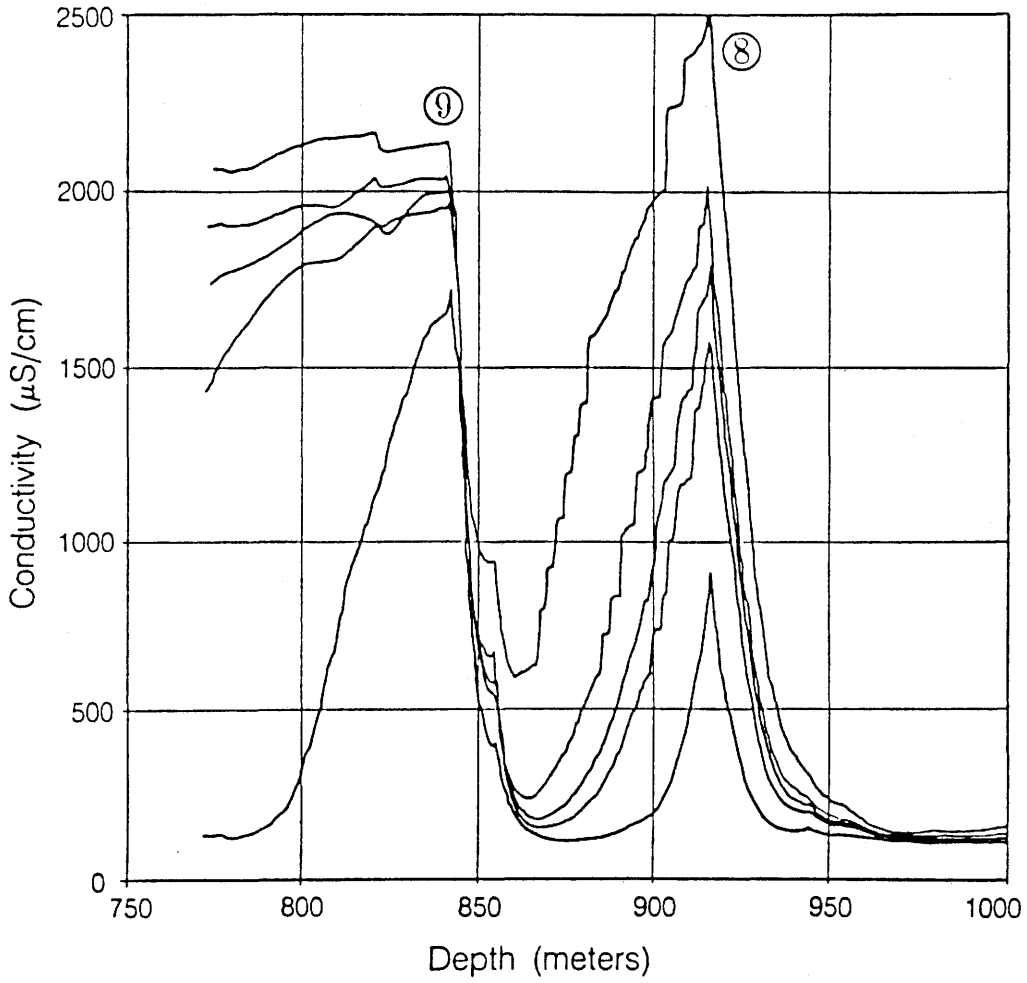


Figure 16: Field fluid-conductivity log data form NAGRA (1986) for the 770-1000 m section of a 1690-m borehole.

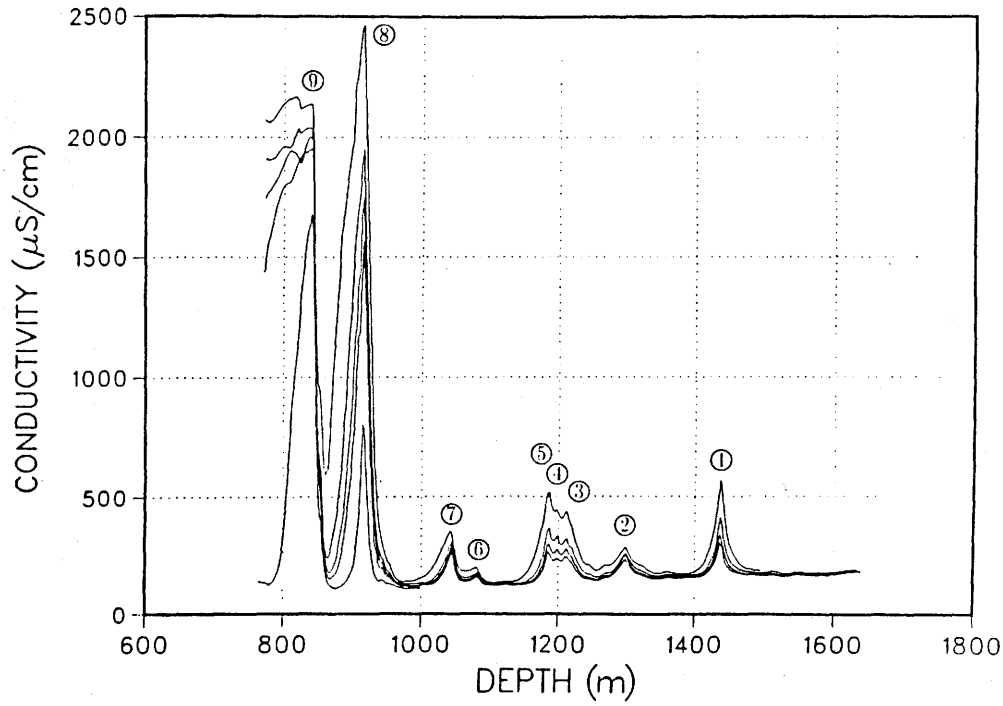


Figure 17: Field fluid-conductivity log data from NAGRA (1986) for the full logged 770-1640 m section of a 1690-m borehole.

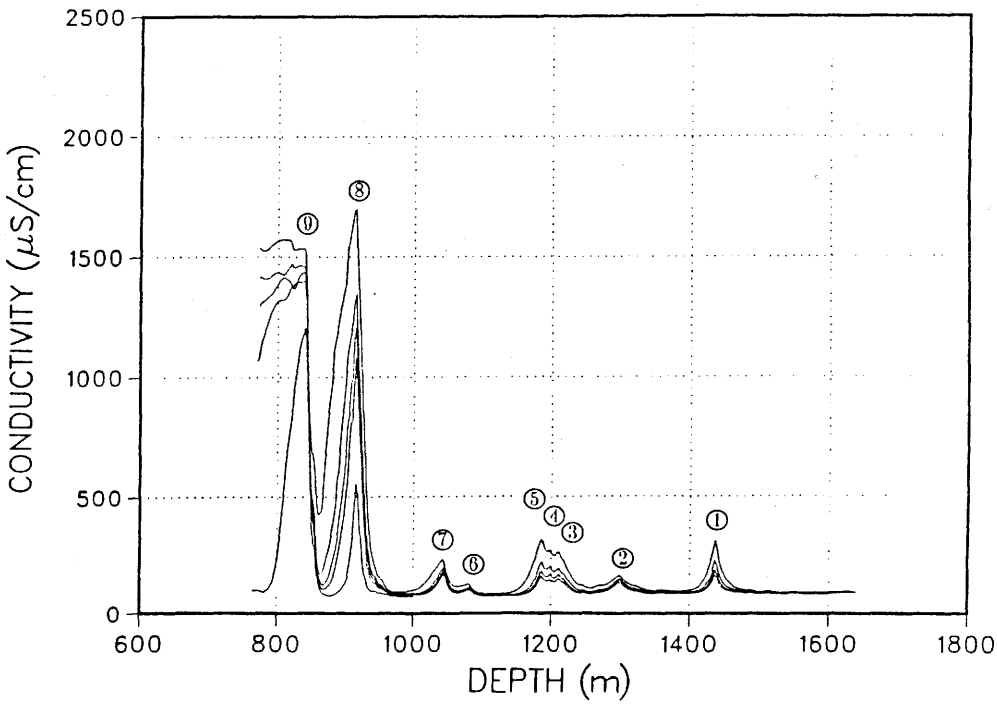


Figure 18: Normalized fluid-conductivity log data.

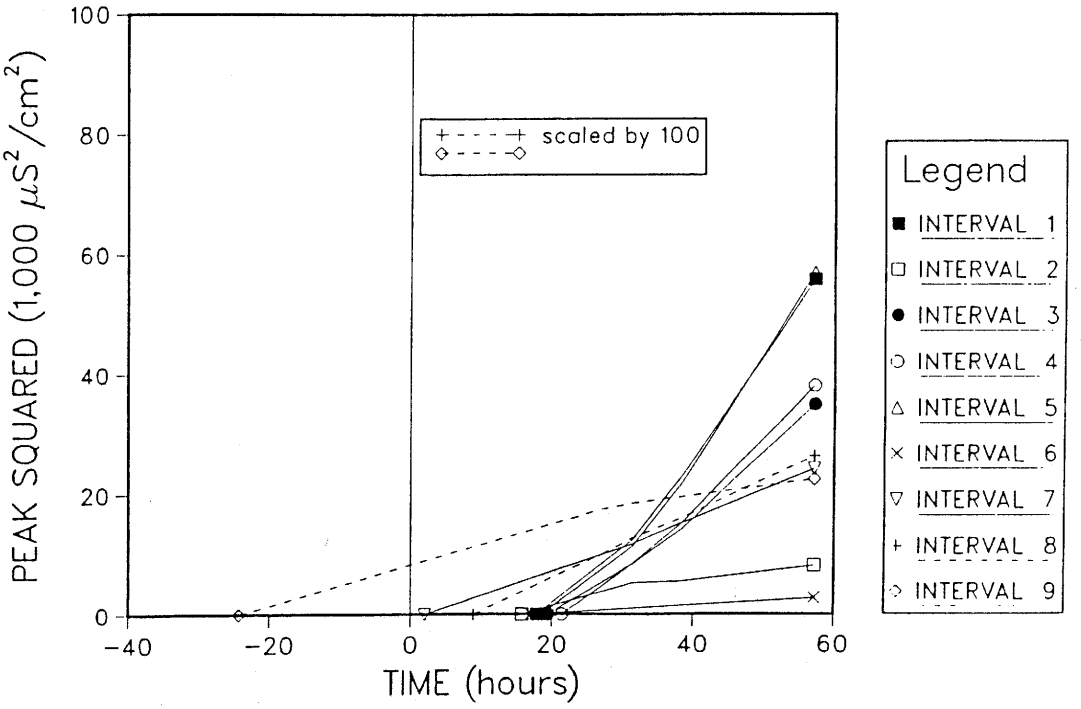


Figure 19: Peak values squared versus time plots for all nine inflow points.

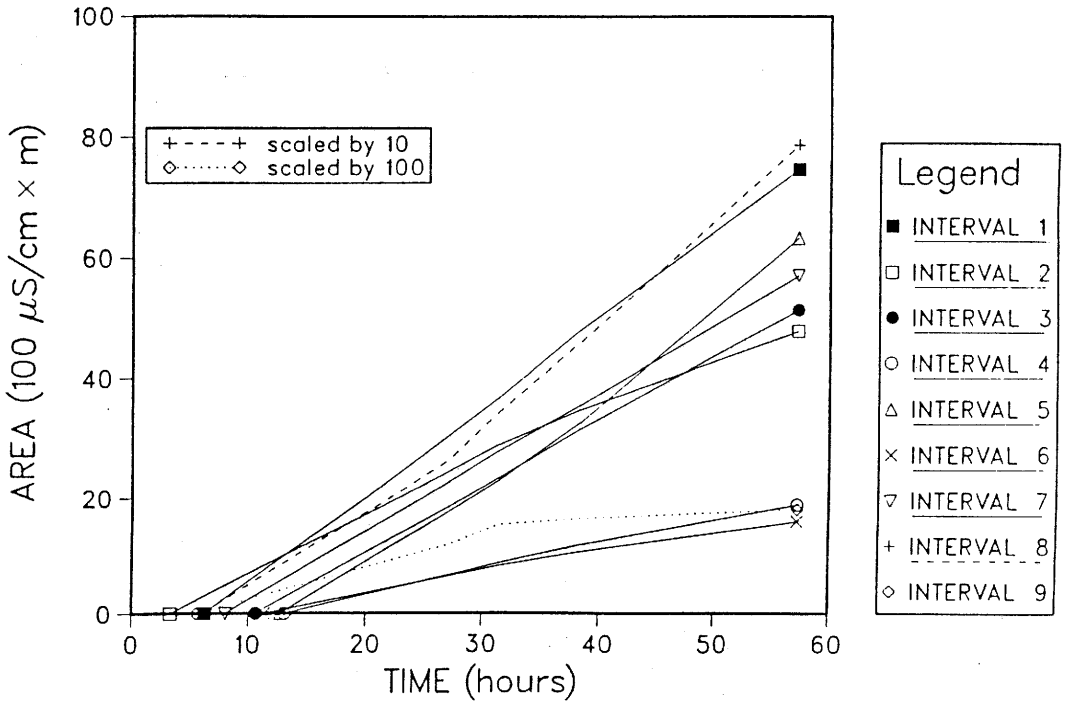


Figure 20: Area versus time plots for all nine inflow points.

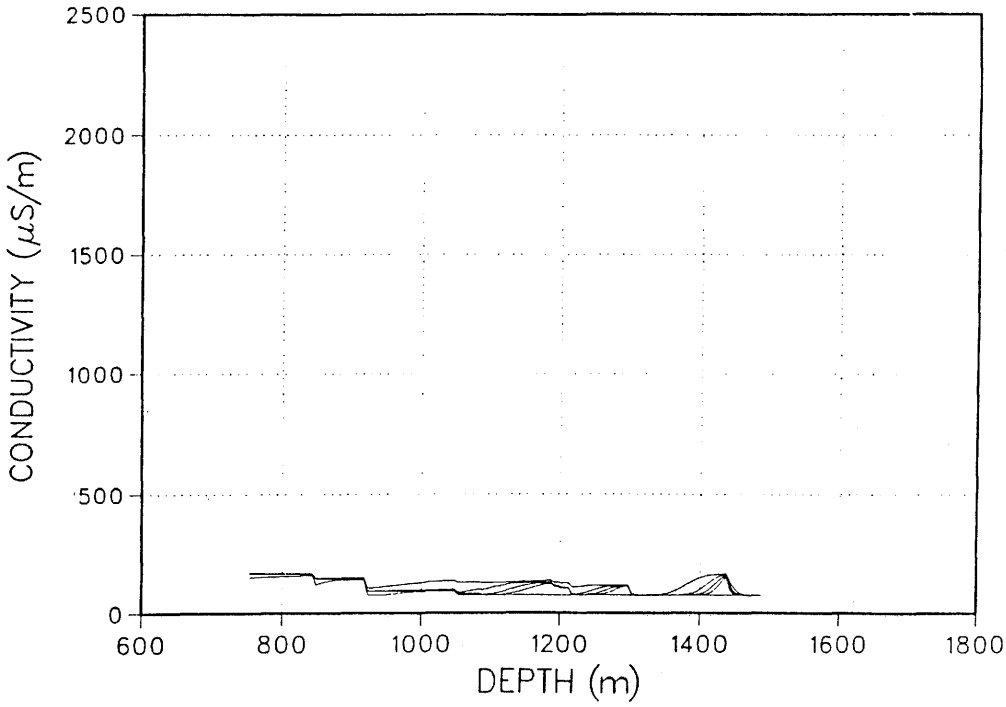


Figure 21: An early attempt to match the field data. The parameters used are given in Table 3. The assumed total flowrate from the borehole section under study was too large.

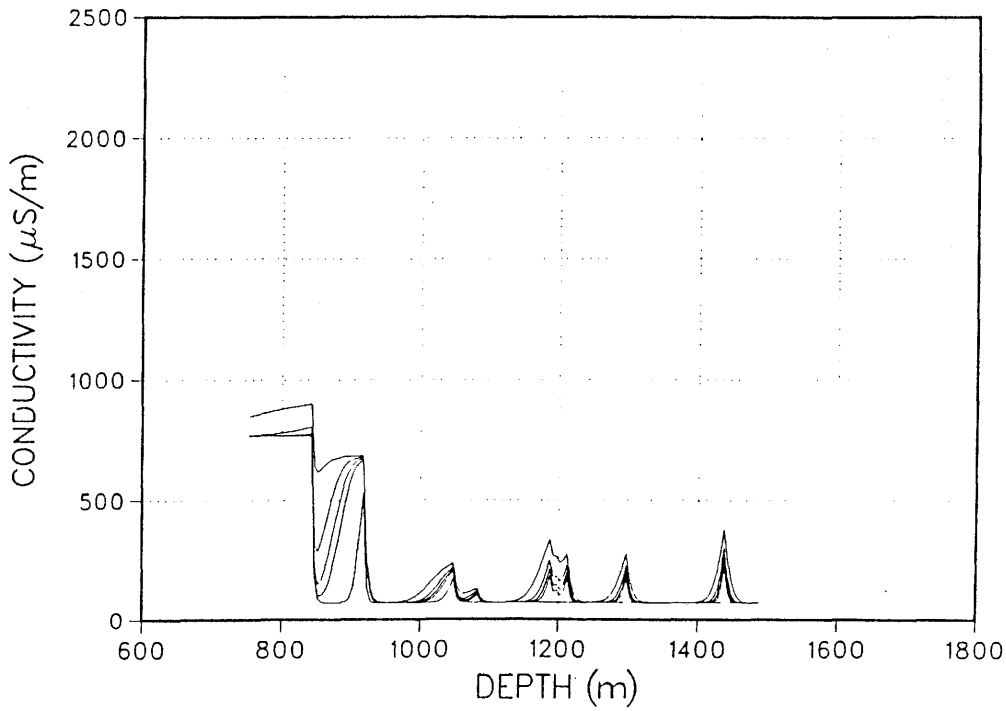


Figure 22: A base case for sensitivity studies. The parameters used are given in Table 4. The curves are for time of 13.03, 27.12, 31.38, 38.41 and 57.24 hours.

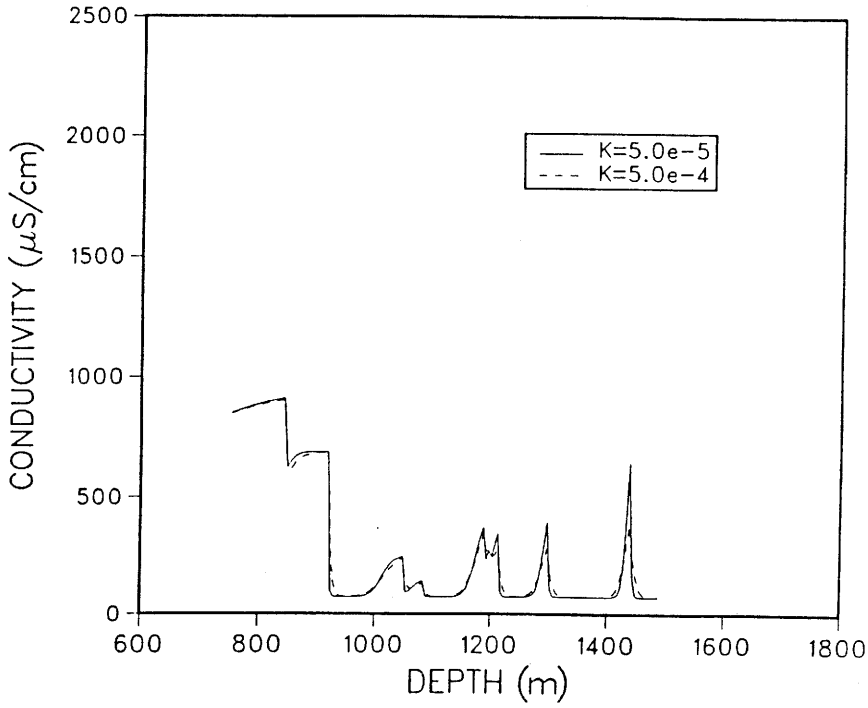


Figure 23: Results if the borehole dispersion coefficient is reduced by a factor of 10 relative to the base case, the other parameters remaining the same. Only results for 57.24 hours are shown. The broken curve is the base case results.

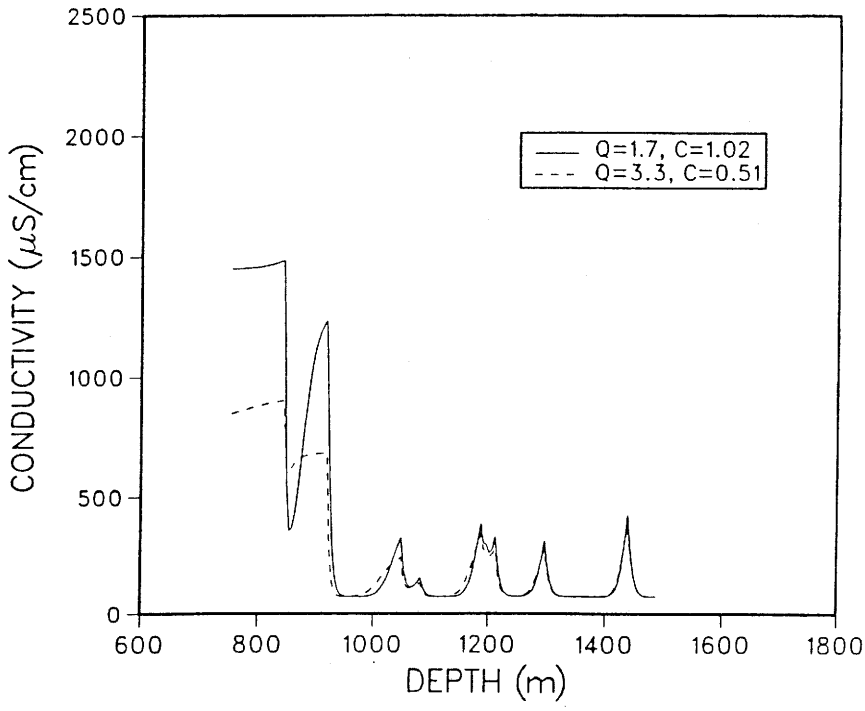


Figure 24: Results at 57.24 hours of sensitivity studies relative to the base case: In the parameters given in Table 3 $q_i C_{oi}$ are kept the same, but all $Q_i$'s are increased by a factor of 2 and all $C_{oi}$'s are decreased by a factor of 2.

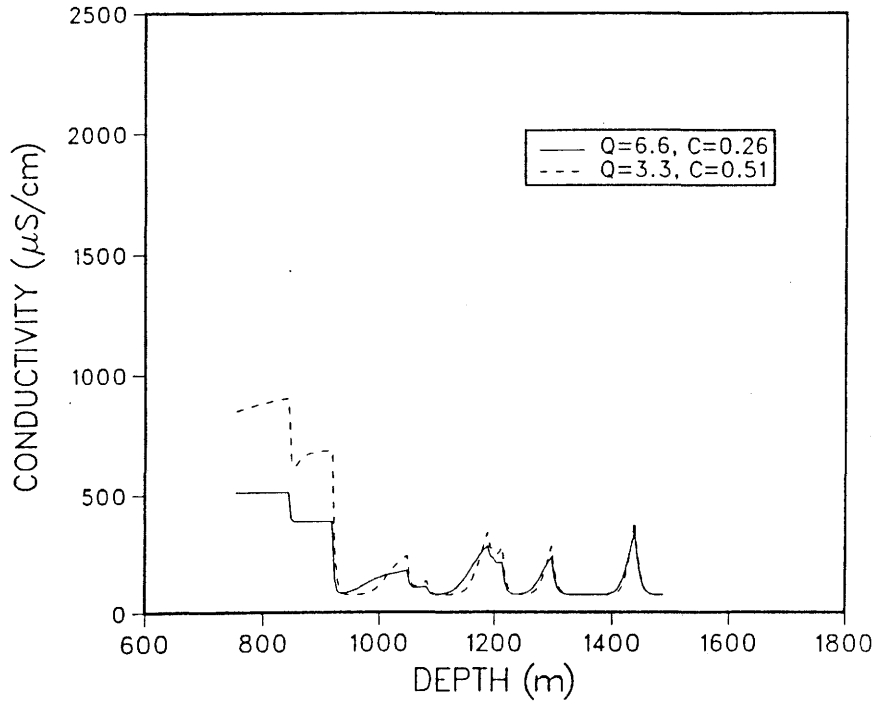


Figure 25: Results at 57.24 hours of sensitivity studies relative to the base case: In the parameters given in Table 3 $q_i C_{oi}$ are kept the same, but all $C_{oi}$'s are increased by factor of 2 and all $q_i$'s are decreased by a factor of 2.

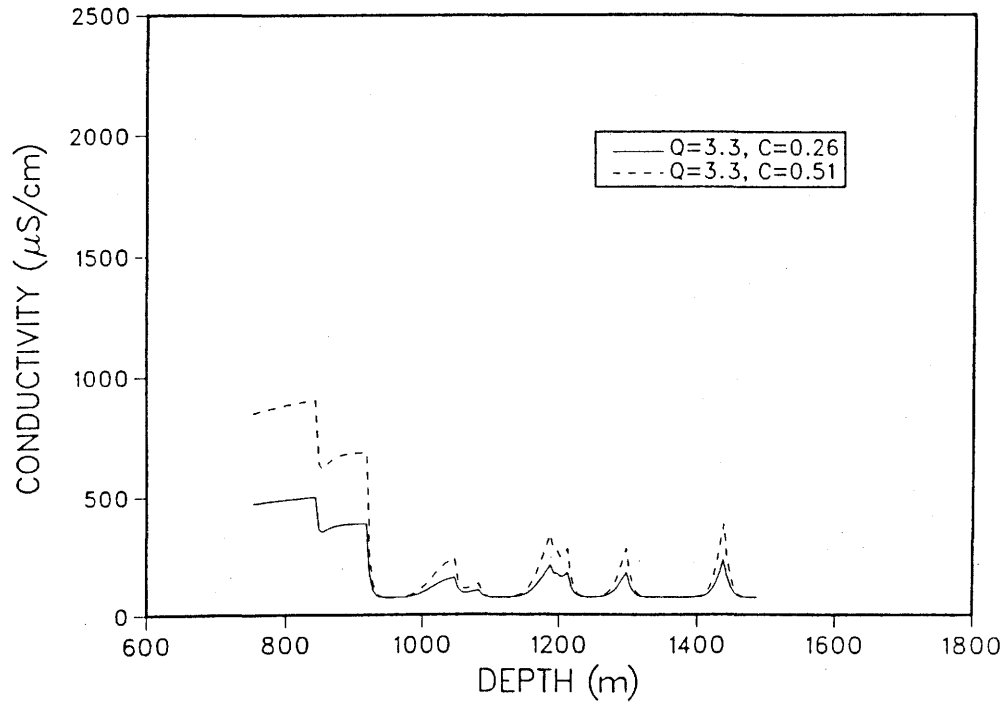


Figure 26: Results at 57.24 hours of sensitivity studies relative to the base case: In the parameters given in Table 3 $q_i C_{oi}$ are kept constant, but all $C_{oi}$ and $q_{oi}$ are reduced by a factor of 2.

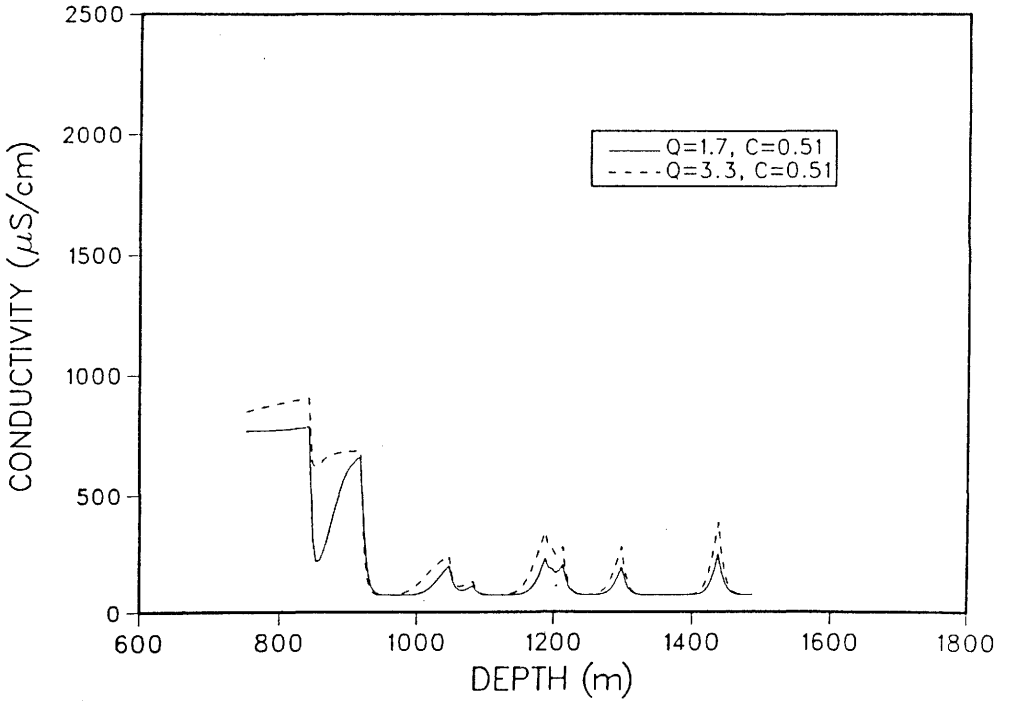


Figure 27: Results at 57.24 hours of sensitivity studies relative to the base case: In the parameters given in Table 3 all $C_{oi}$'s are kept constant, but all $q_i$ and $C_{oi}$ are reduced by a factor of 2.

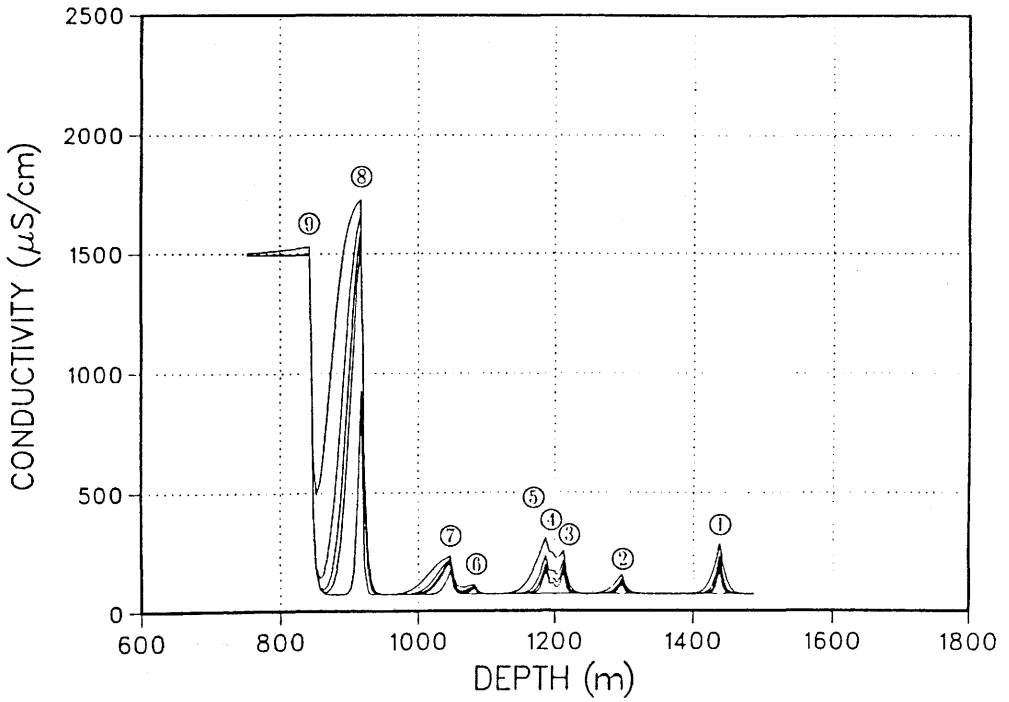


Figure 28: The final match to field data with the parameters given in Table 4, for times = 13.03, 27.12, 31.78, 38.41 and 57.24 hours.

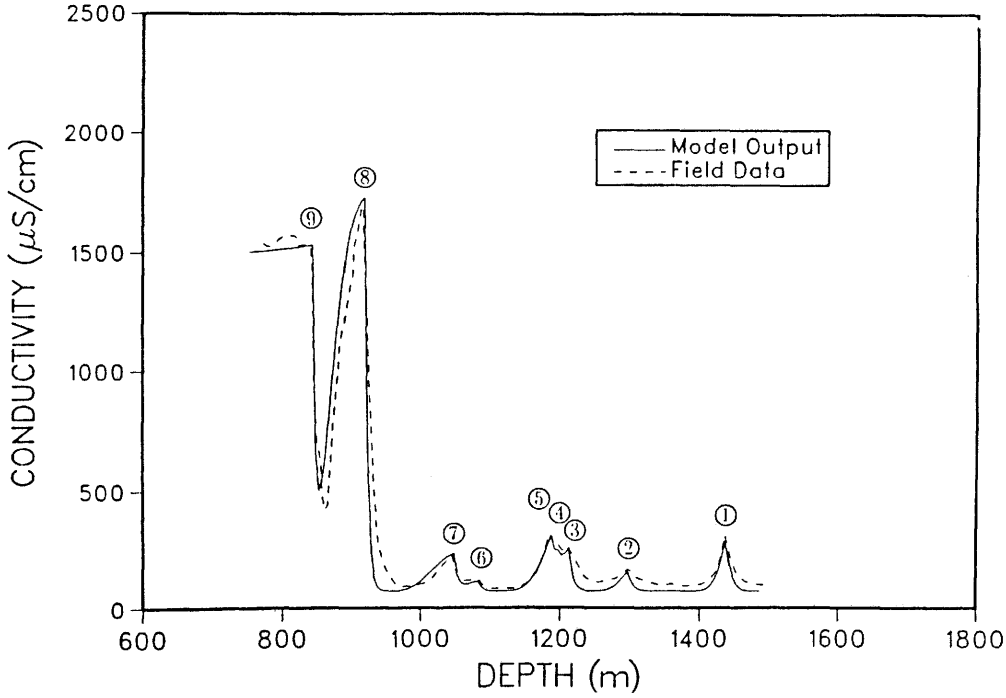


Figure 29: Comparison of field data (dashed lines) and final-matched calculated results (solid lines). Only results at 57.24 hours are shown.

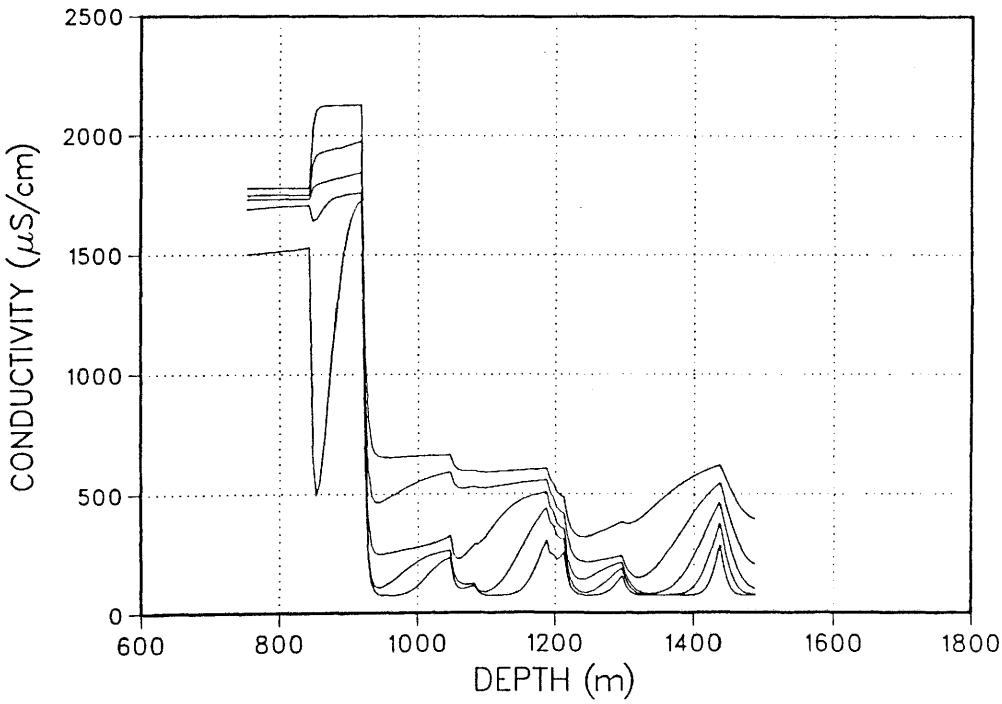


Figure 30: Calculated results at large times (57, 115, 230, 460, 918 hours) based on the final-match parameters given in Table 4.